University of Wisconsin Milwaukee
UWM Digital Commons

Theses and Dissertations

May 2018

3D SEM Surface Reconstruction from Multi-View Images

Waleedur Rehman
University of Wisconsin-Milwaukee

Follow this and additional works at: https://dc.uwm.edu/etd

 Part of the Computer Sciences Commons

Recommended Citation
Rehman, Waleedur, "3D SEM Surface Reconstruction from Multi-View Images" (2018). *Theses and Dissertations*. 1908.
https://dc.uwm.edu/etd/1908

This Thesis is brought to you for free and open access by UWM Digital Commons. It has been accepted for inclusion in Theses and Dissertations by an authorized administrator of UWM Digital Commons. For more information, please contact open-access@uwm.edu.

3D SEM SURFACE RECONSTRUCTION FROM MULTI-VIEW IMAGES

by

Waleed ur Rehman

A Thesis Submitted in

Partial Fulfillment of the

Requirements for the Degree of

Master of Science

in Computer Science

at

The University of Wisconsin-Milwaukee

May 2018

ABSTRACT

3D SEM SURFACE RECONSTRUCTION FROM MULTI-VIEW IMAGES

by

Waleed ur Rehman

The University of Wisconsin-Milwaukee, 2018
Under the Supervision of Professor Zeyun Yu

The scanning electron microscope (SEM), a promising imaging equipment has been used to determine the surface properties such as compositions or geometries of specimens by achieving increased magnification, contrast, and resolution. SEM micro-graphs, however, remain two-dimensional (2D). The knowledge and information about their three-dimensional (3D) surface structures are critical in many real-world applications. Having 3D surfaces from SEM images provides true anatomic shapes of micro-scale samples which allow for quantitative measurements and informative visualization of the systems being investigated. A novel multi-view approach for reconstruction of SEM images is demonstrated in this research project. This thesis focuses on the 3D SEM surface reconstruction from multi-view images. We investigate an approach to reconstruction of 3D surfaces from stereo SEM image pairs and then discuss how 3D point clouds may be registered to generate more complete 3D shapes from multi-views of the microscopic specimen. Then we introduce a method that uses an algorithm called KAZE, which reconstructs 3D surfaces from multiple views of objects. Then Numerous results are presented to show the effectiveness of the presented approaches.

© Copyright by Waleed ur Rehman, 2018
All Rights Reserved

To

My parents,

My brother Naveed,

My wife Afreen,

Specially my Uncle Nadeem Ejaz

And to all the friends who have helped me along the way.

Hopefully someday I can return the favor

TABLE OF CONTENTS

LIST OF FIGURES vii
LIST OF TABLES ix
LIST OF ABBREVIATIONS x
ACKNOWLEDGEMENTS xi
Chapter 1 1
Introduction 1
1.1. Background and Problem Statement 1
1.2. The Scanning Electron Microscope 1
1.2.1. Secondary Electron Images and Backscattered Electron Images 3
1.3. 3D Surface Reconstruction 4
1.4. 3D Surface Reconstruction from SEM Images 5
1.4.1. Single View Approach 5
1.4.2. Multi-View Approach 6
1.4.3. Hybrid Approach 6
Chapter 2 8
3D SEM Reconstruction from Multiple Views 8
2.1. Introduction 8
2.2. Procedure 11
2.2.1. Overview 11
2.2.2. Image Rectification 13
2.2.3. Patchmatch 17
2.2.3.1. Disparity Test Value [-40 40] 18
2.2.3.2. Disparity Test Value [-10 10] 20
2.2.3.3. Disparity Test Value [-30 30] 23
2.2.4. Point Cloud Generation and Registration 27
2.3. Results 30
2.4. Conclusion 35
Chapter 3 36
Global Approach: Regard3D 36
3.1. Introduction to Regard3D 36
3.2. KAZE Algorithm 37

3.3. A-KAZE 37
3.4. Obtaining a 3D Model 38
3.4.1. Feature Point Detection 38
3.4.2. Key-point Matching 38
3.4.3. Triangulation 38
3.4.4. Densification 39
3.4.5. Surface Generation 39
3.5. Pipeline 40
3.6. Results 41
3.6.1. Dataset 1: Kermit 41
3.6.2. Dataset 2: Der Hass 44
3.7. Other Low Detail 3D Reconstructions 48
3.8. Conclusion 49
Chapter 4 50
Conclusions 50
4.1. Conclusions and Future Work 50
References 53

LIST OF FIGURES

Figure 1 SEM Schematic https://nau.edu/cefns/labs/electron-microprobe/glg-510-class-notes/instrumentation/ 2
Figure 2 (a) View 1 of Tapetal Cell of Arabidopsis Thaliana http://selibcv.org/3dsem/; (b) View 2 of Tapetal Cell of Arabidopsis Thaliana http://selibcv.org/3dsem/ 12
Figure 3 (a) Rectified view 1 of Tapetal Cell of Arabidopsis; (b) Rectified view 2 of Tapetal Cell of Arabidopsis 12
Figure 4 (a) Pseudoscorpion Left View https://www.sciencedirect.com/science/article/pii/S0968432817303128; 14
Figure 5 (a) Pseudoscorpion Left View 30 Strongest Surf Points; (b) Pseudoscorpion Right View 30 Strongest Surf Points 14
Figure 6 Pseudoscorpion Matched Points between Left View and Right View 15
Figure 7 (a) Pseudoscorpion Left View Rectified; (b) Pseudoscorpion Right View Rectified 16
Figure 8 Pseudoscorpion Composite of Left View and Right View 16
Figure 9 (a) Left View Image Initialization Step [-40 40]; (b) Right View Image Initialization Step [-40 40] 18
Figure 10 Left View Image Propagation Step [-40 40] 18
Figure 11 Right View Image Propagation Step [-40 40] 19
Figure 12 Left View Image Refinement Step [-40 40] 19
Figure 13 Right View Image Refinement Step [-40 40] 19
Figure 14 (a) Left View Image Disparity Map [-40 40]; (b) Right View Image Disparity Map [-40 40] 20
Figure 15 (a) Left View Image Initialization Step [-10 10]; (b) Right View Image Initialization Step [-10 10] 20
Figure 16 Left View Image Propagation Step [-10 10] 21
Figure 17 Right View Image Propagation Step [-10 10] 21
Figure 18 Left View Image Refinement Step [-10 10] 21
Figure 19 Right View Image Refinement Step [-10 10] 22
Figure 20 (a) Left View Image Disparity Map [-10 10]; (b) Right View Image Disparity Map [-10 10] 22
Figure 21 (a) Left View Image Initialization Step [-30 30]; (b) Right View Image Initialization Step [-30 30] 23
Figure 22 Left View Image Propagation Step [-30 30] 23
Figure 23 Right View Image Propagation Step [-30 30] 24
Figure 24 Left View Image Refinement Step [-30 30] 24
Figure 25 Right View Image Refinement Step [-30 30] 24
Figure 26 (a) Left View Image Disparity Map [-30 30]; (b) Right View Image Disparity Map [-30 30] 25
Figure 27 3D Surface Reconstruction of Pseudoscorpion SEM Stereo Pair 28
Figure 28 Sparse 3D Reconstructed Pseudoscorpion Surface 29
Figure 29 Dense 3D Surface of Pseudoscorpion using Point Cloud Registration 30
Figure 30 Hexagon TEM Copper Grid Dataset http://selibcv.org/3dsem/ 30
Figure 31 Reconstructed 3D Model without Point Cloud Registration Hexagon TEM Copper Grid Dataset 31
Figure 32 Reconstructed 3D Model with Point Cloud Registration Hexagon TEM Copper Grid Dataset 31
Figure 33 Pollen Grain from Brassica Rapa Dataset http://selibcv.org/3dsem/ 32

Figure 34 Reconstructed 3D Model without Point Cloud Registration Pollen Grain from Brassica Rapa Dataset 32
Figure 35 Reconstructed 3D Model with Point Cloud Registration Pollen Grain from Brassica Rapa Dataset 33
Figure 36 TEM Copper Grid Dataset http://selibcv.org/3dsem/ 33
Figure 37 Reconstructed 3D Model without Point Cloud Registration Pollen Grain from TEM Copper Grid Dataset 34
Figure 38 Reconstructed 3D Model with Point Cloud Registration Pollen Grain from TEM Copper Grid Dataset 34
Figure 39 Kermit Dataset 11 Images Montage 41
Figure 40 Matching Results from Kermit Dataset 42
Figure 41 Dense Point Cloud Generation from Triangulated Points Kermit 42
Figure 42 Generated Surface from 11 Images Kermit Dataset 43
Figure 43 Der Hass Dataset 79 Images Montage 44
Figure 44 Matching Results From Der Hass Dataset 45
Figure 45 Dense Point Cloud Generation from Triangulated Points Der Hass 45
Figure 46 Generated Surface from 79 Images Der Hass Dataset 46
Figure 47 Low Detail 3D Model Reconstruction of Objects From 3 Images 48
Figure 48 Low Detail 3D Model Reconstruction of Human Face with 30 Images 48

LIST OF TABLES

Table 1 Comparison of the Secondary Electron and Backscattered Electron imaging in a SEM 3
Table 2 Comparison Between Computational Time Required by CPU and GPU Implementation of the Patchmatch Stereo Algorithm; http://selibcv.org/3dsem/; https://www.sciencedirect.com/science/article/pii/S0968432817303128 26
Table 3 Step by Step Running Time for Each Dataset 47

LIST OF ABBREVIATIONS

SEM – Scanning Electron Microscope/Scanning Electron Microscopy

SFS – Shape from Shading

PS – Photometric Stereo

SFM – Structure from Motion

FED – Fast Explicit Diffusion

LIOP – Local Intensity Order Pattern

SE – Secondary Electron

BSE – Backscattered Electron

SIFT – Scale-Invariant Feature Transform

SURF – Speeded Up Robust Features

ACKNOWLEDGEMENTS

I would like to extend my gratitude to many of the UWM Faculty. First, I would like to thank professor Zeyun Yu for acting as my advisor for this thesis and for recognizing my capabilities and giving me this amazing opportunity to work with him on this project. He also helped me develop my graphics and programming skills required for this thesis and many more projects. His constant motivation and expert guidance enabled me to successfully complete this study.

I am also grateful to professor Seyed H. Hosseini and professor Ichiro Suzuki, who agreed to be on my evaluation committee with a rather short amount of notice.

I also extend gratitude to Ahmadreza Baghaei and Ahmed P. Tafti, whose previous research in the field was of great help to me, and serves as the primary motivation for the SEM reconstruction and registration implemented for this thesis.

Finally, I will also offer my thanks to Benjamin Newman and Tianfang LI, who were close friends during my time at UW-Milwaukee and spurred me on to try my best within the past year.

This thesis and its contents as is, are solely for nonprofit educational use. Reference to this thesis, if it or its contents are used in future works, is requested, and highly appreciated.

Chapter 1

Introduction

1.1. Background and Problem Statement

3D surface reconstruction from a set of 2D images has been an active research area in the field of computer vision. The technique of Scanning Electron Microscope (SEM) imaging has also been traditionally used in various research areas to view the surface structure of microscopic samples. However, SEM images remain two-dimensional (2D). Having three-dimensional (3D) shapes from 2D SEM images would provide anatomic surfaces allowing for quantitative measurements and informative visualization of the objects being investigated. Many facets of science have benefited and could further benefit from 3D SEM surface reconstruction techniques. In computer science tremendous amount of work is available on algorithm designing and software developing of 3D surface reconstruction from 2D images.

1.2. The Scanning Electron Microscope

A scanning electron microscope (SEM) is used to generate surface images of a specimen on a microscopic level. It does this by scanning a specimen with a beam of high energy electrons in an optical column. The electrons emitted by the beam then interact with the atomic structure of the specimen and generate topographic images. The beam is generated in a vacuum by the electron gun. The electron gun comprises of three main components; filament, shield and an anode. The filament serves as the source of electrons for the beam. The shield functions to direct the emitted electrons in a downward trajectory in the column of the microscope. The

anode is for drawing electrons down into the column at a constant speed. This electron column uses magnetic electron lenses on the sides of the column to project an image of the electron beam onto the specimen. Throughout the length of the column, the beam is de-magnified by a factor of 100 to 1000 times its original size and is focused on the specimen.

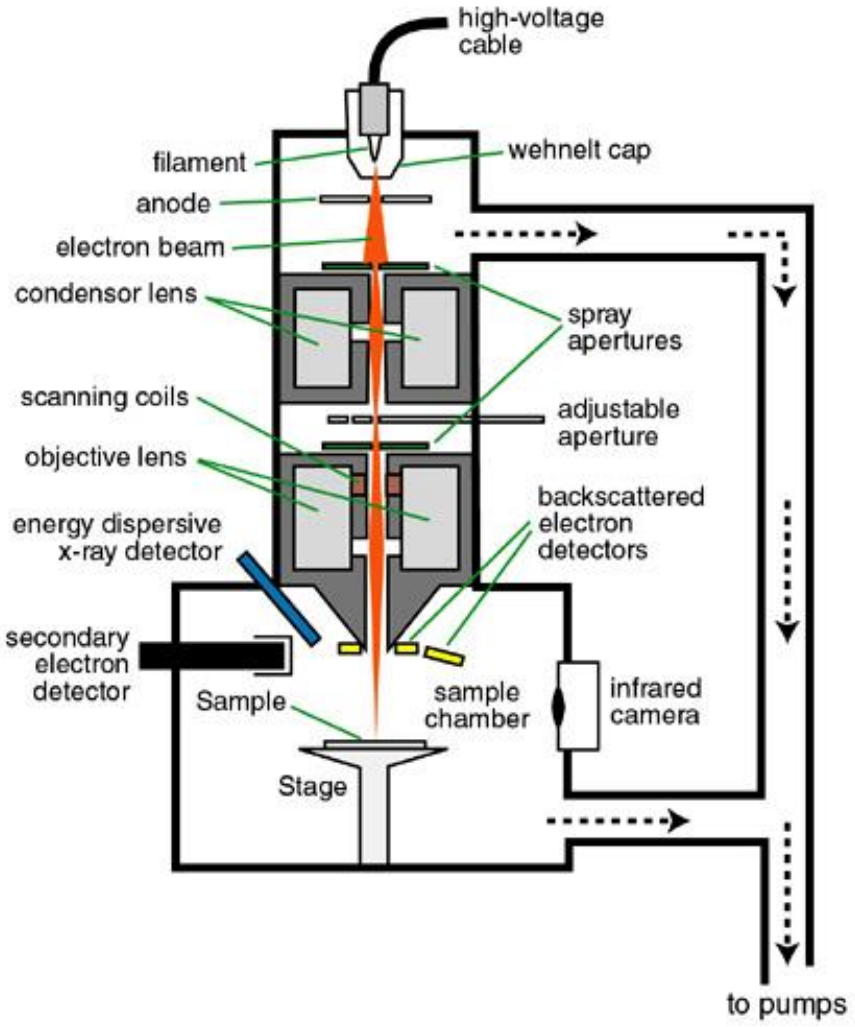

Figure 1 SEM Schematic *https://nau.edu/cefns/labs/electron-microprobe/glg-510-class-notes/instrumentation/*

1.2.1. Secondary Electron Images and Backscattered Electron Images

The reflection of secondary electrons is helpful in creating the topographic imagery of a sample. Secondary electrons (SEs) are created when electrons are ejected due to impact with the electron beam. The secondary electrons are distinguished from the backscattered electrons as they have much lower energies.

Backscattered electrons (BSEs) are mainly used to learn about the composition of the sample and have energies much higher than the secondary electrons. The backscattering of electrons occurs as a result of multiple deflections through small angles on a sample. BSEs are scattered from the sample with little energy loss and are able to travel greater depths within the sample.

Like the SE emissions, the BSE emissions are also affected by the angle of the surface. The detector 'sees' different electrons produced from various angles on the surface and a topographic image can be generated. However, the topographic image produced by BSEs tends to have a lower resolution than that produced by SE emission.

Table 1 Comparison of the Secondary Electron and Backscattered Electron imaging in a SEM

SE Based Imaging	BSE Based Imaging
Higher resolution	Lower resolution
Darker intensities	Brighter intensities
Inelastic scattering (low energy electrons)	Elastic scattering (high energy electrons)
Contains topographical information	Contains compositional information

1.3.3D Surface Reconstruction

3D surface reconstruction techniques constitute an important part of 3D computer vision. It has been used in the process of creating 3D models from only a set of 2D images. The origin of 3D computer vision dates to 1957 when Gilbert Hobrough illustrated a method and designed the apparatus for analog implementation of stereo image correlation. In 1963, Larry Roberts proposed the first 3D surface reconstruction technique by introducing a machine perception algorithm which could create and display 3D geometry information of objects from a single two-dimensional photograph. In 1970, B. P. Horn designed another 3D surface reconstruction technique called Shape-from-Shading (SFS) which used shading from an individual image to calculate the surface orientation. In 1977, R. J. Woodham designed the Photometric Stereo (PS) algorithm which was a multi-view version of the Shape-from-Shading. In 1990, C. Tomasi and T. Kanade estimated 3D surface structure from a sequence of 2D images. The method they proposed is now popularly known as called Structure from Motion (SFM). In 2002, T. Zickler, P. N. Belhumeur, and D. Kriegman designed Helmholtz stereopsis to reconstruct the 3D geometry of an object from a collection of 2D images. In 2011, J. Shotton et al. provided a new method to predict 3D positions of body joints from a single depth image in a fast and accurate manner by recording the shape of the reflected points of light by means of a camera. Instead of temporal information, this was known as structured light capture. This technique has famously been used in Microsoft's Kinect accessory.

1.4.3D Surface Reconstruction from SEM Images

The process of creating a 3D shape model of a microscopic sample is still not quite easy to solve since its three-dimensional shape in the real world is only projected into and available as 2D digital images. Over the past years, there has been an expansion in the designing and development of 3D surface reconstruction algorithms for images obtained by a SEM. These algorithms can be categorized into three main classes:

1) Single-View

2) Multi-View

3) Hybrid

1.4.1. Single View Approach

In the Single-View approach, a set of 2D images from a single view point with varying light directions are used for 3D SEM surface reconstruction. Photometric Stereo is the main algorithm used in this class to produce 3D geometry information of a microscopic sample. Photometric Stereo is a 3D computer vision algorithm which rapidly computes the three-dimensional geometry of an object by examining 2D images that are being viewed from the same viewpoint, but being illuminated from different directions. The Photometric Stereo method has five general steps:

1) Take a set of single view digital images of an object under different light directions.

2) Determine the light directions.

3) Calculate surface normal.

4) Calculate reflection coefficient.

5) Estimate depth.

1.4.2. Multi-View Approach

In the Multi-View approach, a 3D computer vision algorithm is used, namely Structure from Motion (SFM). This method utilizes stereo pairs taken by tilting the microscopic object between photographs. Structure from Motion is established on the theory of projective geometry, with considering different perspectives from different view angles to restore the 3D structure of a specific object. By using corresponding feature points or key points in the image pairs, a 3D point can be reconstructed by linear triangulation. Basic requirements are the determination of camera calibration (intrinsic camera parameters) and camera's rotation and translation. The SFM method has five major steps:

1) Take a set of digital images of an object.

2) Identify key points or feature points in the images that can be detected in other images in the set.

3) Search for corresponding points in images which is also known as point-matching.

4) Estimate camera projection matrices.

5) Compute 3D surface model by using linear triangulation.

1.4.3. Hybrid Approach

The third class of 3D SEM surface reconstruction algorithms is called the Hybrid method, and it offers a compromise between the Single-View and the Multi-View approaches. This approach uses an algorithm to reconstruct surfaces and 3D images by applying stereo and shading information from two 2D images. Since the shape from shading does the

reconstruction very well when the 2D data has homogeneous texture, the stereo and shading information are complementary requirements of the reconstruction, and shape from stereo helps when there are various features in the data.

Chapter 2

3D SEM Reconstruction from Multiple Views

2.1.Introduction

Scanning electron microscope (SEM) is one the principal research and industrial equipment for imaging on the microscopic scale. SEM and its diverse applications have been a very active research over the decade, and scientific studies well covered the use of SEM in broad domains ranging from biomedical applications to materials sciences and Nano-technologies. SEM is an advanced microscopy device that produces high quality images of microscopic specimens using a focused beam of electrons which can be then captured by two types of detectors, secondary electron (SE) and backscattered electron (BSE) detectors, to provide both compositional and/or geometrical information. However, SEM micrographs remain 2D while the need for having a more quantitative knowledge of the 3D shape/surface of the microscopic samples is of high importance. The techniques used for this purpose can be categorized into three major classes: a) single-view, b) multi-view, and c) hybrid strategies. In single-view approaches, using varying lighting directions on a single perspective, a group of 2D SEM images are captured and utilized for 3D SEM surface modeling. In multi-view strategies, on the other hand, a set of 2D SEM images from different perspectives assists the 3D SEM surface reconstruction process. While each technology carries its own cons and pros, the hybrid mechanisms try to combine single-view and multi-view algorithms to restore a 3D shape model from 2D SEM images.

The Photometric Stereo as the major strategy in the single-view class tries to estimate the surface normal vectors of the microscopic sample by observing the object being illuminated

from different directions. Paluszynski et al. designed a single-view 3D surface modeling approach based on the Photometric Stereo algorithm which also incorporates advanced signal processing algorithms along with both SE and BSE detectors to restore the 3D shape model of SEM images. Pintus et al. developed an automatic alignment strategy for a four-source Photometric Stereo technique for reconstructing the depth map of SEM specimen. Kodama et al. designed a genetic algorithm to tackle the topographical surface reconstruction problem of SEM based on Photometric Stereo method. The proposed genetic algorithm has been applied to the line profile reconstruction from the signals captured by both SE and BSE detectors. Vynnyk et al. proposed a Photometric Stereo based algorithm to 3D SEM surface reconstruction and studied the efficiency of SEM detector system towards a 3D modeling. Slowko et al. designed a Photometric Stereo based algorithm to reconstruct the 3D surface model of SEM micrographs with the use of angular distribution of back-scattered electron emission to achieve a digital map of surface elevations. This contribution examined different SEM environmental conditions as a high vacuum SEM which was equipped with the BSE detector system utilized for 3D surface reconstruction.

The multi-view class is one of the most promising class of methods for 3D surface modeling of SEM images. It is based on acquisition of multiple images from different perspectives. The Structure from Motion (SfM) and Stereo Vision algorithms are advanced visual computational methods which consider feature-points matching for accurate 3D SEM surface reconstruction. The class of multi-view 3D reconstruction approaches can be categorized into two major classes: a) sparse feature-based approaches and b) dense pixel based approaches. While methods from the first class are employed to establish a set of robust matches between an

image pair or a set of images based on sparsely placed distinct feature-points, dense multi-view techniques try to discover matches for all points in the images. These matches along with other computational methods will then be used to accurately estimate the projective geometry and 3D surface models. Raspanti et al. presented a high resolution dense multi-view method for 3D reconstructions of biological samples obtained by a SEM. The work implemented novel solutions including a neural adaptive point matching technique to tackle the problem of dense 3D reconstruction. Samak et al. developed a SfM based algorithm to restore 3D surface model of SEM micrographs. The proposed method initialized a set of 3D points from 2D corresponding points and then triangulated the obtained 3D points into the 3D surface mesh with a mapped texture on the shape model. Carli et al. evaluated the uncertainty of stereo vision algorithm for the problem of 3D SEM surface modeling. Uncertainty for different cases of tilt and rotation were discussed in the work and a relative uncertainty equal to 5% and 4% was achieved for the case of rotation and tilt respectively. Zolotukhin et al. studied the pros and cons of SfM algorithm focusing on two-view 3D SEM surface reconstruction problem. Tafti et al. reviewed the state of the art 3D SEM surface reconstruction solutions, addressing several enhancements for the research study, and developed a sparse mutli-view algorithm to tackle 3D SEM surface modeling problem. Using machine learning solutions and adaptive strategies, Tafti et al. proposed an improved sparse feature-based multi-view method which outperforms their earlier work in terms of accuracy and computation demands. Marinello et al. analyzed and studied the 3D reconstruction of SEM images based on different instrumental configurations including calibration, title-angle, magnification etc.

In single-view 3D surface reconstruction, creating a full model of the microscopic sample is not possible since the images are limited to only one view-point. Moreover, recreating the SEM micrographs of the sample under different illumination conditions is difficult. On the other hand, multi-view approaches offer a more general and achievable framework for the task.

2.2.Procedure

2.2.1. Overview

The overview of the proposed work is almost the same as described in the previously for the multi-view approach. Scattered electron based images are used in the approach since we are interested in the reconstruction of the surface of the microscopic specimen. These multi-view image datasets are captured by using a SEM device with computer controlled specimen stage. From this dataset a pair of images (stereo pair) is selected and then Epipolar rectification using sparse SURF features done to ensure a more horizontally-concentrated disparity variation. This is followed by dense correspondence between the pixels which provides the one-to-one correspondence between the matching points of the two images.

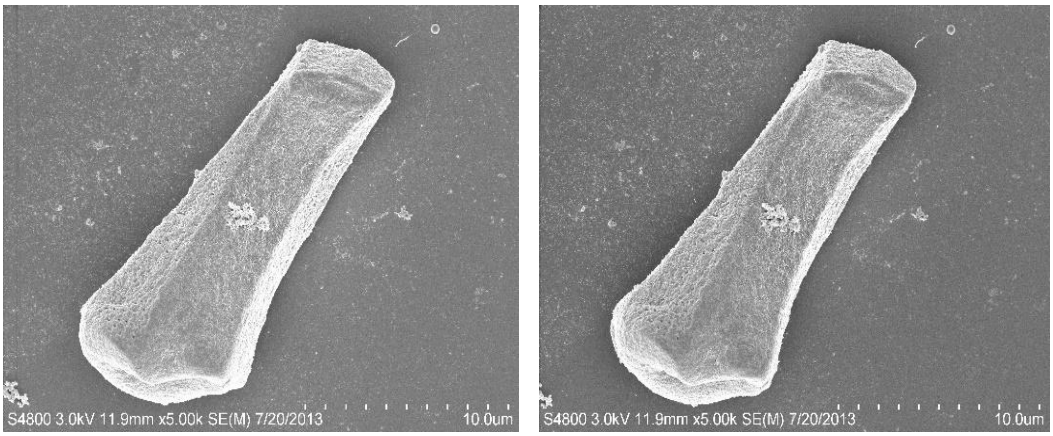

(a) **(b)**

Figure 2 (a) View 1 of Tapetal Cell of Arabidopsis Thaliana *http://selibcv.org/3dsem/*; (b) View 2 of Tapetal Cell of Arabidopsis Thaliana *http://selibcv.org/3dsem/*

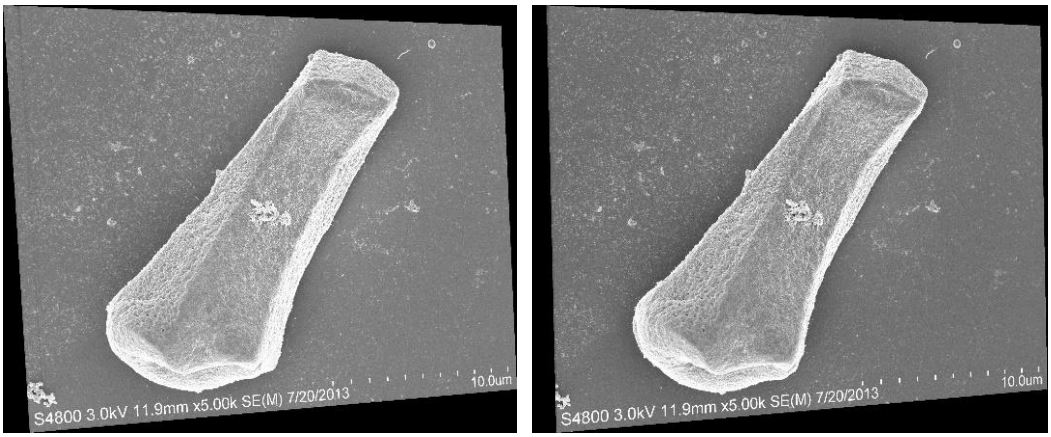

(a) **(b)**

Figure 3 (a) Rectified view 1 of Tapetal Cell of Arabidopsis; (b) Rectified view 2 of Tapetal Cell of Arabidopsis

Once the images are rectified, the Patchmatch Stereo algorithm is used to generate depth maps from which 3D point cloud can be generated for the purpose of reconstruction. This process is repeated for other images of the same sample taken at different angles and similarly other point clouds are generated and then registered. The registration of these points clouds can be done manually as well by simply loading the point clouds and using the basic computer vision

functions of translation and rotation. For manual registration the corresponding points must be selected between the point clouds and then using translation and rotation overlapped with each other. The approach in the research used is the Iterative Closest Point Algorithm. In the following subsections each of the steps are elaborated in more detail.

2.2.2. Image Rectification

Image rectification is a transformation process used to project images onto a common image plane. It is used in computer stereo vision to simplify the problem of finding matching points between images known as the correspondence problem.

In an image there can be various objects, and from these objects some feature points can be extracted to provide a feature description for the object. This feature description is used to identify this object in the other images of the dataset.

The feature point extraction and their matching is one of the key point in the process of image rectification. The feature point matching can be done by either of the following feature detectors: SIFT (Scale-Invariant Feature Transform) or SURF (Speeded Up Robust Features).

The feature detector used in this approach is SURF which is a local feature detector and descriptor. The main reason for choosing SURF over SIFT is that it is several times faster than SIFT and is also more robust against different image transformations (as claimed by its authors). The SURF algorithm is based on the same principles as SIFT but it varies in each step. The algorithm has three parts: 1) Interest point detection, 2) Local neighborhood detection and 3) Matching.

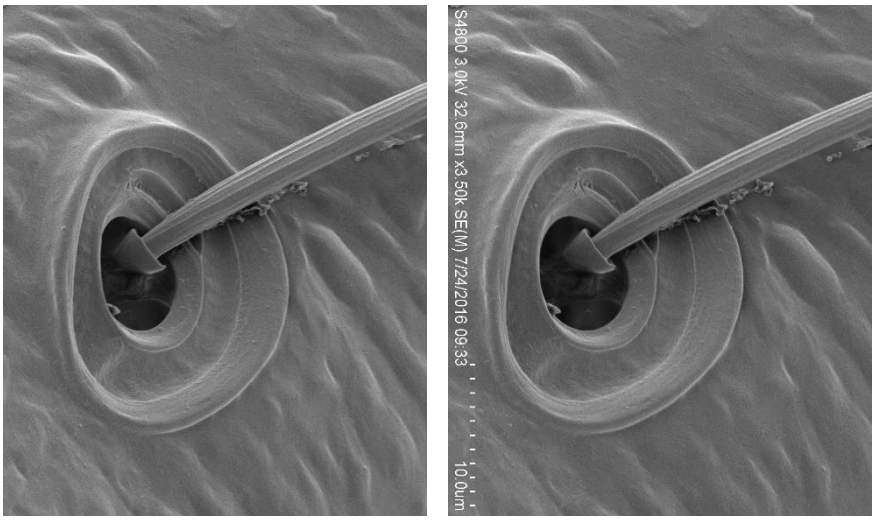

(a) **(b)**

Figure 4 (a) Pseudoscorpion Left View
***https://www.sciencedirect.com/science/article/pii/S0968432817303128*;**

(b) Pseudoscorpion Right View
https://www.sciencedirect.com/science/article/pii/S0968432817303128

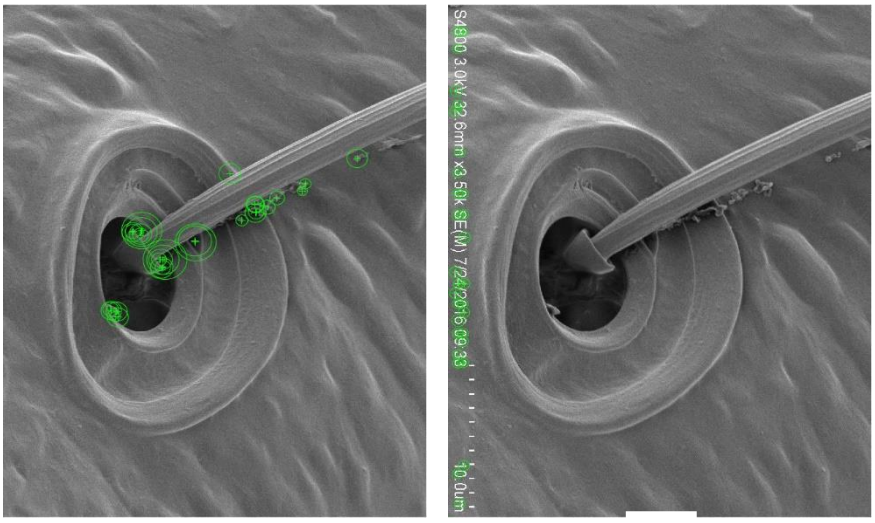

(a) **(b)**

Figure 5 (a) Pseudoscorpion Left View 30 Strongest Surf Points; (b) Pseudoscorpion Right View 30 Strongest Surf Points

The figure 5(a) and figure 5(b) shows the step where strongest feature/key points are detected for both the images that are provided input to the algorithm. After this detection the correspondence between the two images is found using these feature/key points.

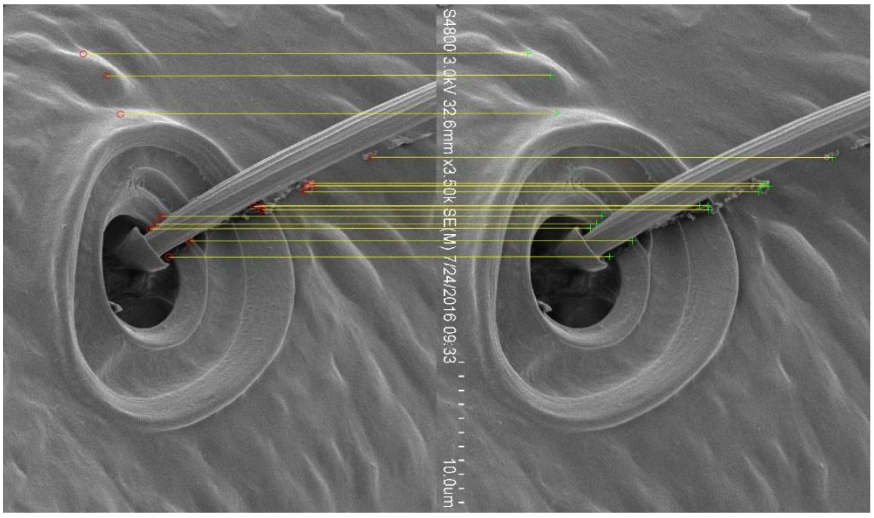

Figure 6 Pseudoscorpion Matched Points between Left View and Right View

The points matched between the two views can be clearly seen from the figure 6 above. With this point correspondence the images can be rectified and then all these epipolar lines will be parallel in the rectified image plane. The result can be seen below in figure 7(a) and figure 7(b).

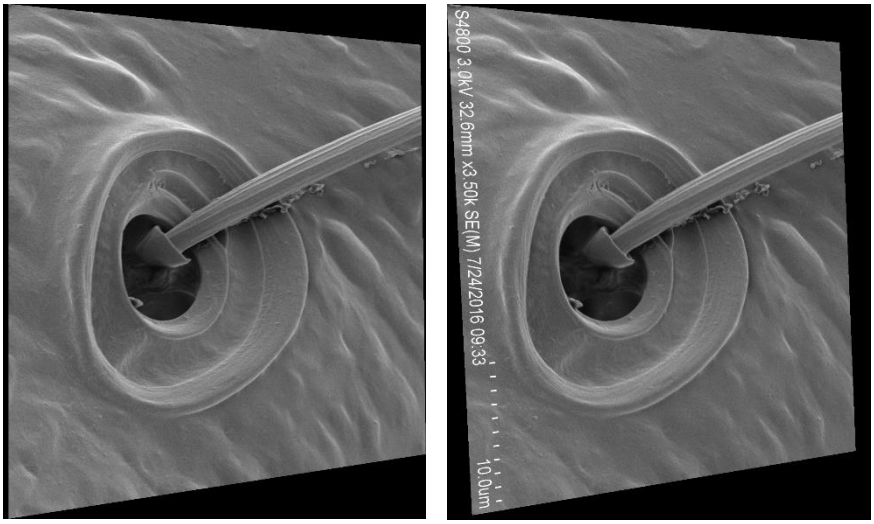

(a) (b)

Figure 7 (a) Pseudoscorpion Left View Rectified; (b) Pseudoscorpion Right View Rectified

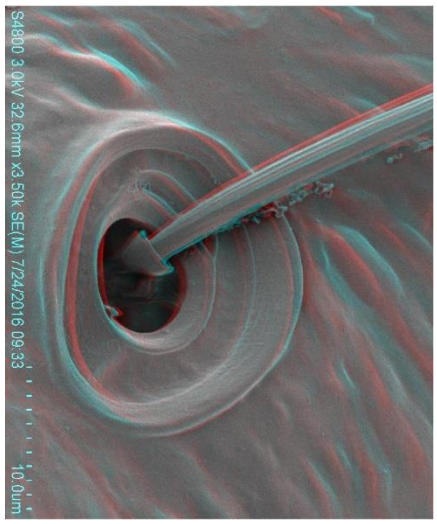

Figure 8 Pseudoscorpion Composite of Left View and Right View

By combining the figure 7(a) and figure 7(b) we get figure 8 which is said to be the composite of both the images. It is more like an overlapping of the images in cyan and red color to identify the difference between the two.

Followed by this process comes the process for evaluating the disparity values and finding the depth map for the given stereo pair. This is achieved by using the Patchmatch algorithm.

2.2.3. Patchmatch

In order to find correspondence between patches (usually small regions) between the images, the Patchmatch algorithm is often used. The algorithm takes a stereo pair of images as input (thus also called Patchmatch Stereo Algorithm). Then it defines a nearest-neighbor field (NNF). The Patchmatch Stereo algorithm is iterative and works in three steps: 1) Initialization, 2) Propagation, 3) Refinement.

A straightforward implementation i.e. CPU based implementation of the Patchmatch Stereo algorithm consumes a large amount of time. For this approach a GPU implementation has been used which enabled much faster computing of the disparity maps for the input stereo image pair. The algorithm takes two rectified images as its input. Along with this rectified stereo image pair user needs to define the disparity value range (minimum disparity and maximum disparity). This disparity value range can have significant effect on the resulting 3D models. Not only this the range also affects the total computing time of the implementation. Also patch radius and patch stride values must be provided by the user to proceed. Otherwise a default value of 10 for patch radius and 1 for patch stride is selected which in most cases works fine. To observe the effect of disparity values on the results, 3 different value ranges were used that can be seen in the figures provided below.

2.2.3.1. Disparity Test Value [-40 40]

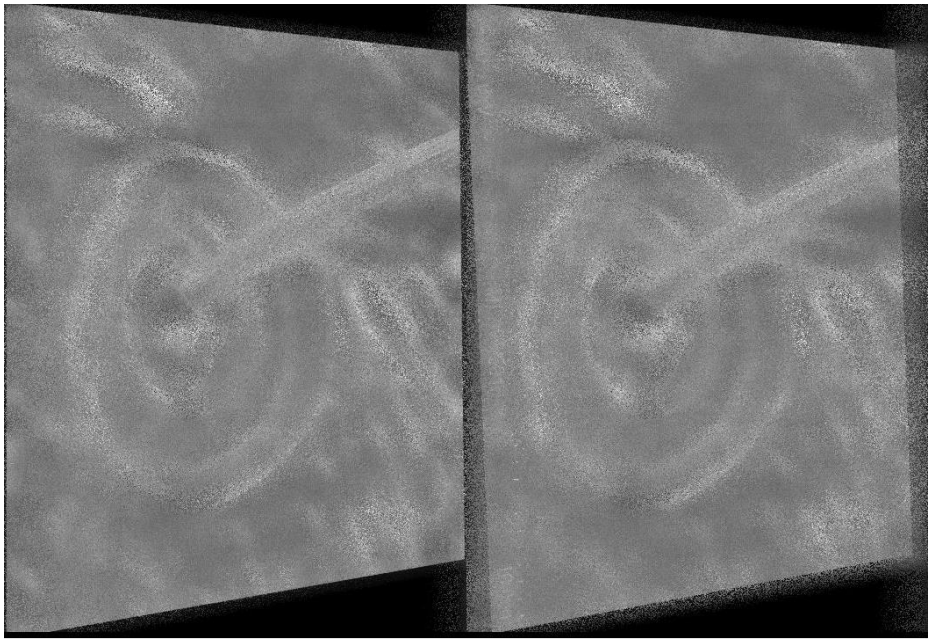

(a) (b)

Figure 9 (a) Left View Image Initialization Step [-40 40]; (b) Right View Image Initialization Step [-40 40]

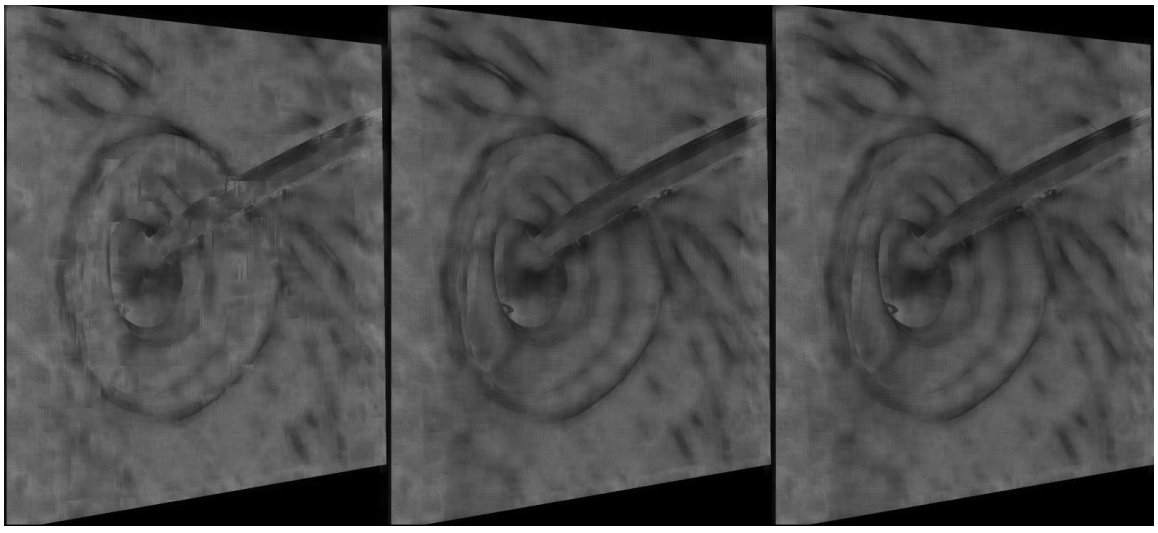

Figure 10 Left View Image Propagation Step [-40 40]

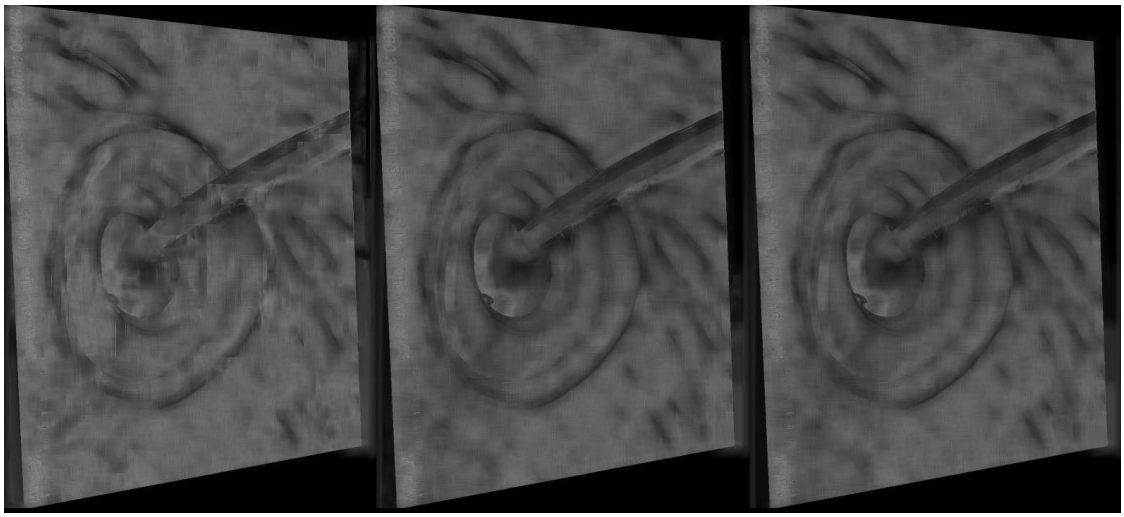

Figure 11 Right View Image Propagation Step [-40 40]

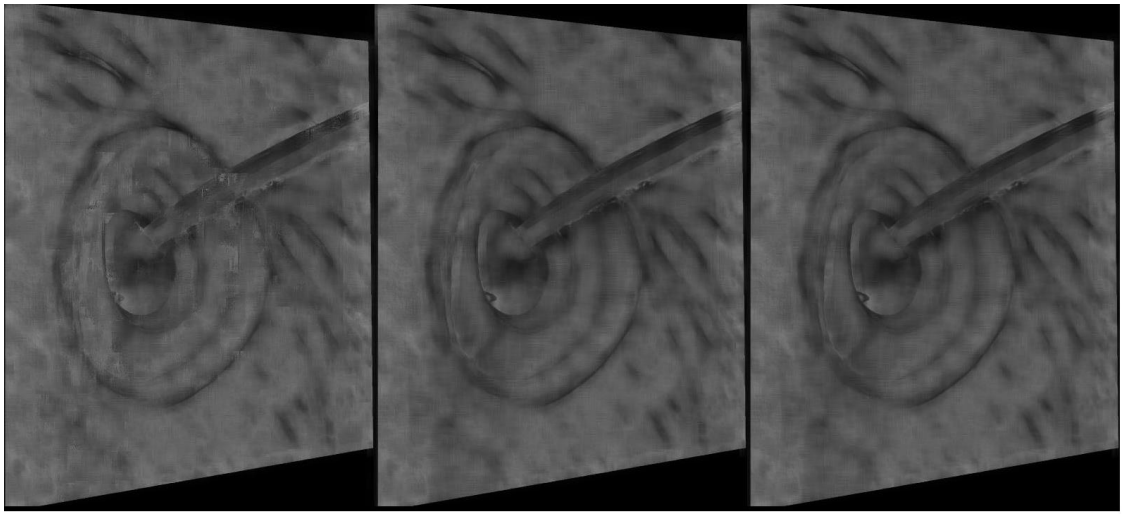

Figure 12 Left View Image Refinement Step [-40 40]

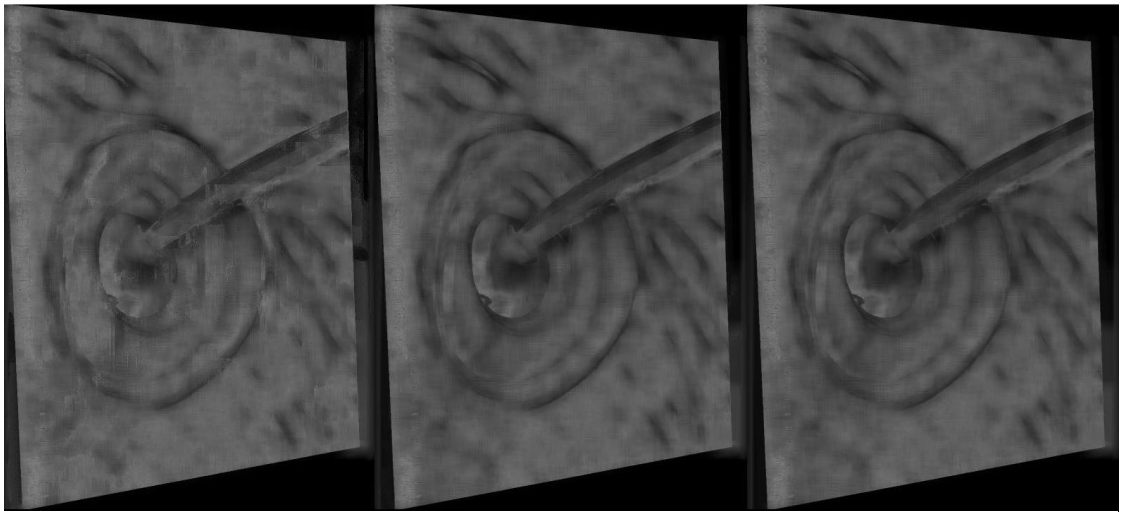

Figure 13 Right View Image Refinement Step [-40 40]

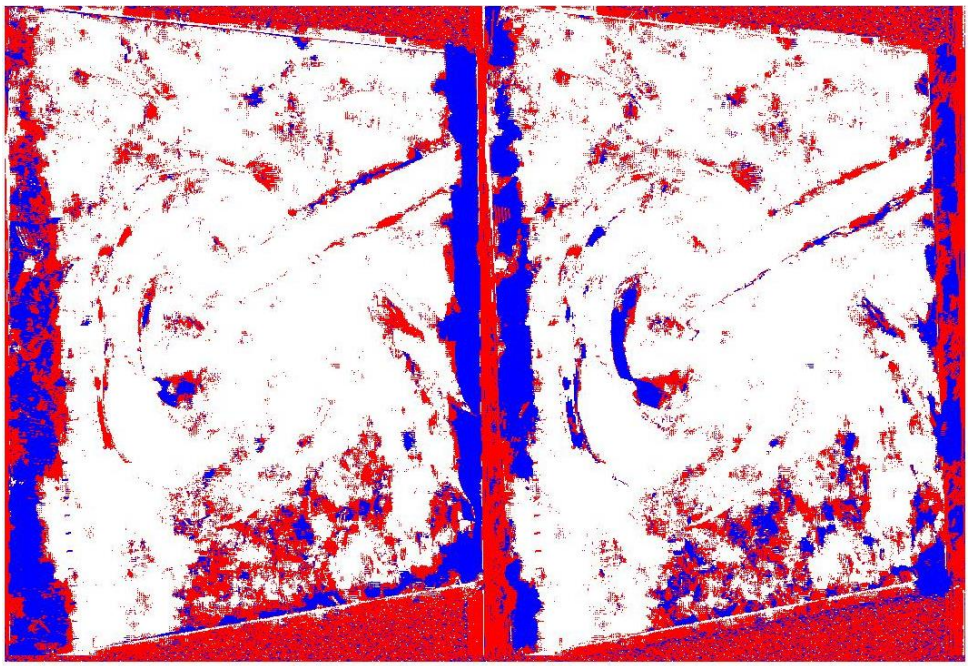

(a) (b)

Figure 14 (a) Left View Image Disparity Map [-40 40]; (b) Right View Image Disparity Map [-40 40]

2.2.3.2. Disparity Test Value [-10 10]

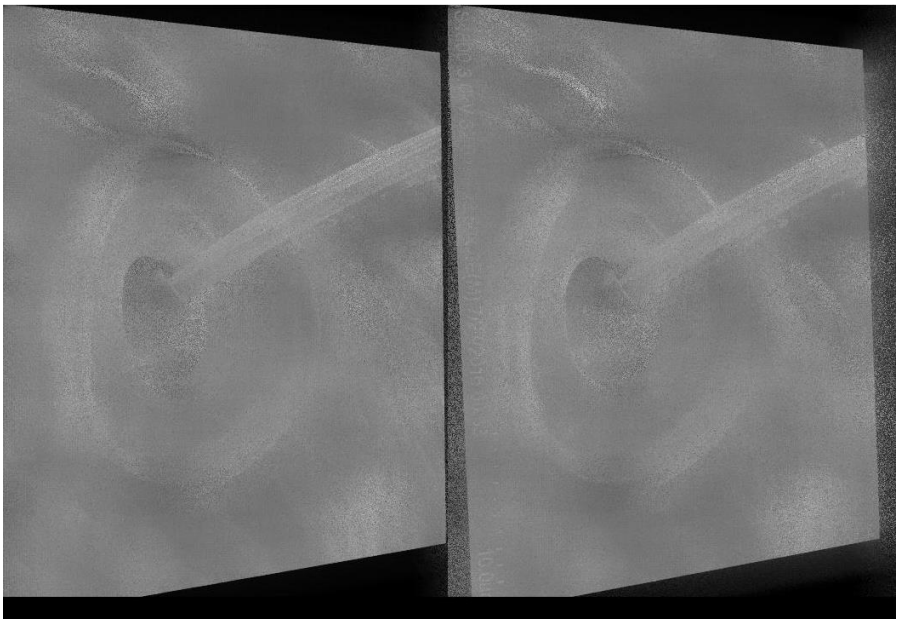

(a) (b)

Figure 15 (a) Left View Image Initialization Step [-10 10]; (b) Right View Image Initialization Step [-10 10]

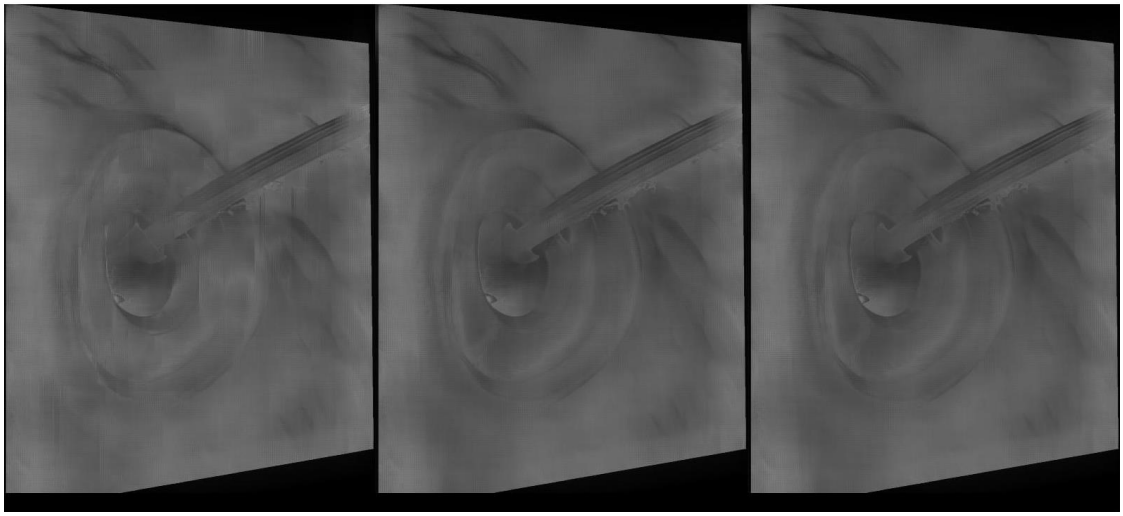

Figure 16 Left View Image Propagation Step [-10 10]

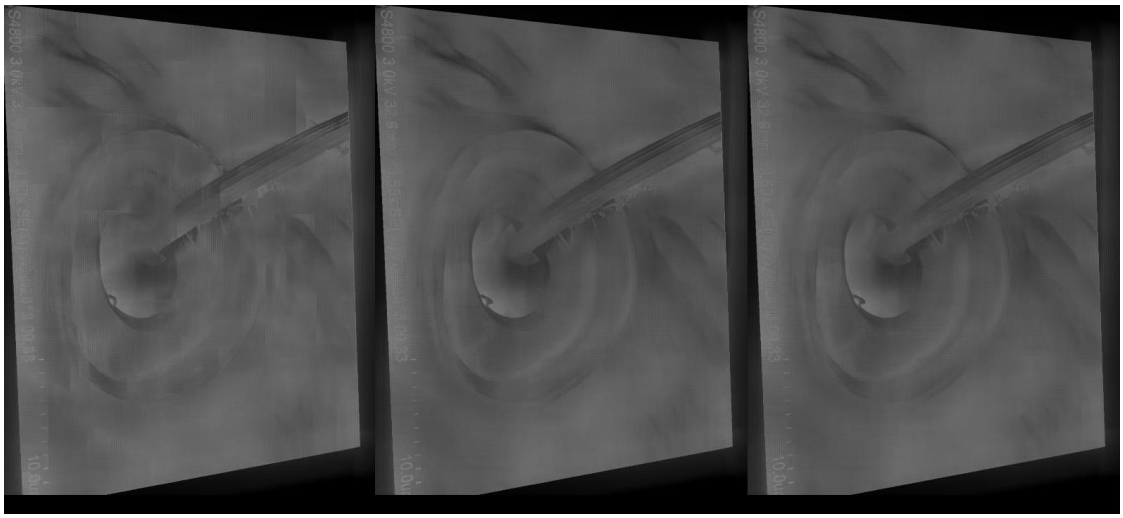

Figure 17 Right View Image Propagation Step [-10 10]

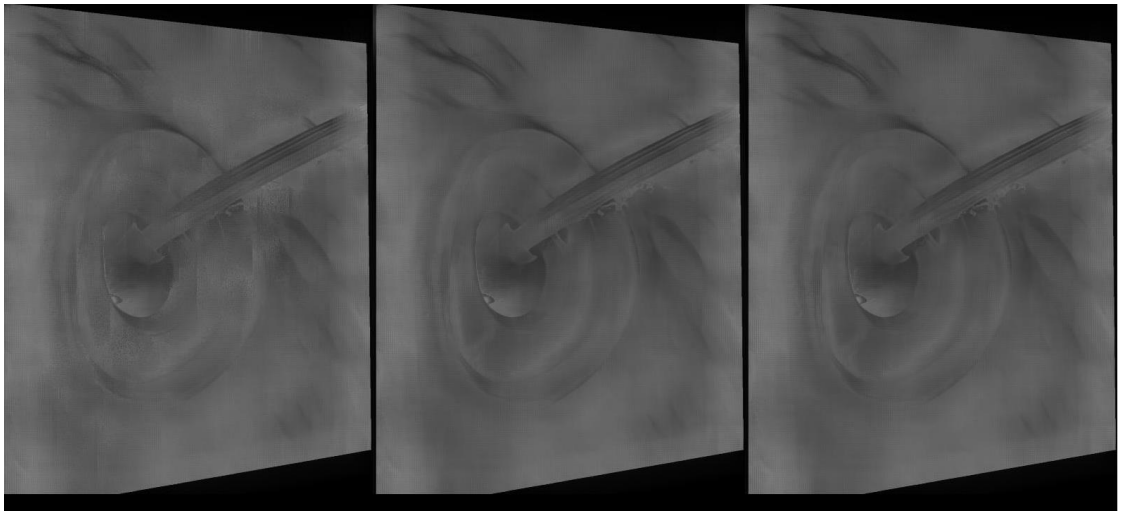

Figure 18 Left View Image Refinement Step [-10 10]

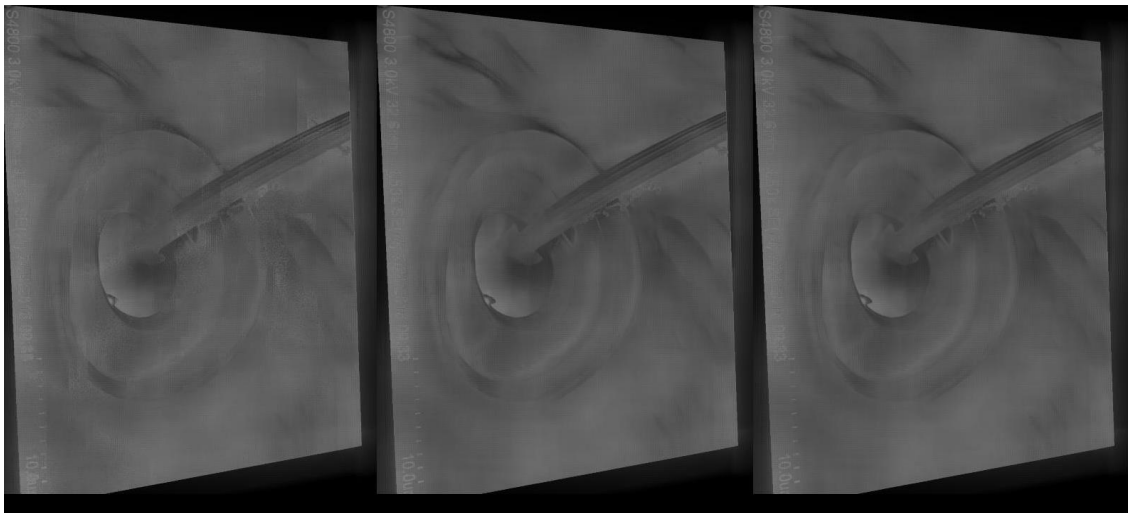

Figure 19 Right View Image Refinement Step [-10 10]

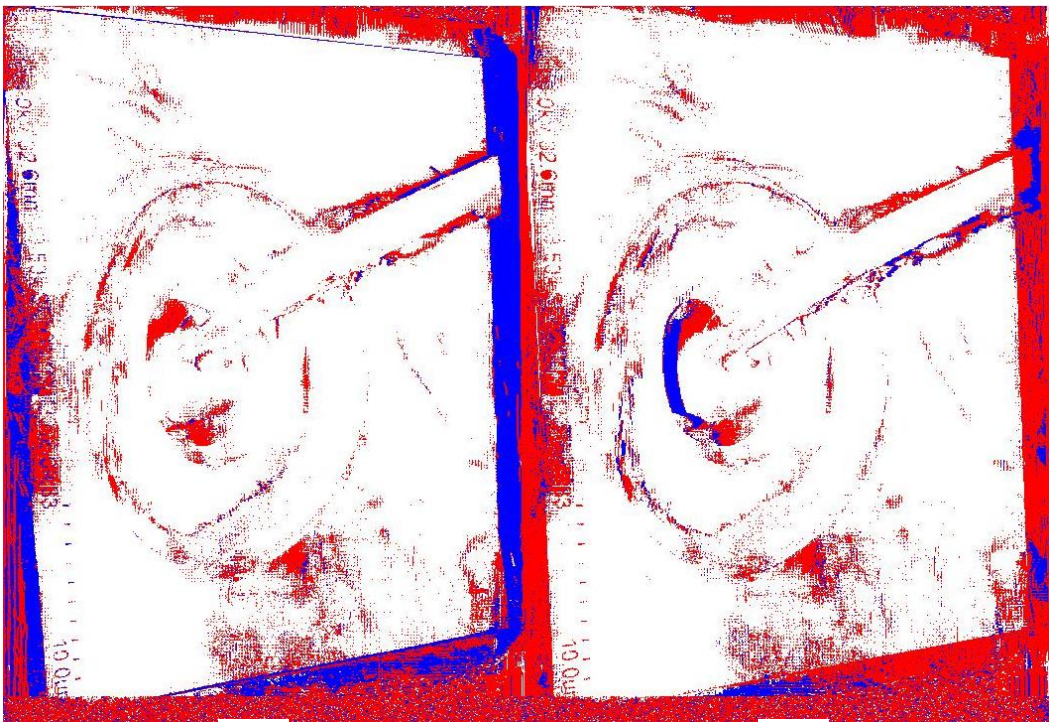

(a) (b)

Figure 20 (a) Left View Image Disparity Map [-10 10]; (b) Right View Image Disparity Map [-10 10]

2.2.3.3. Disparity Test Value [-30 30]

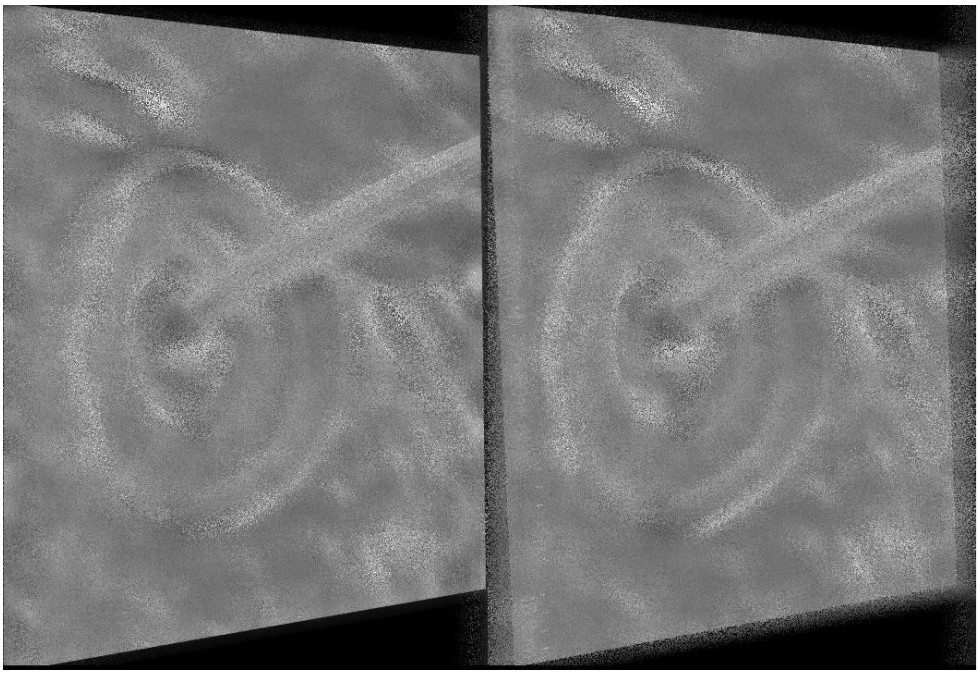

(a) (b)

Figure 21 (a) Left View Image Initialization Step [-30 30]; (b) Right View Image Initialization Step [-30 30]

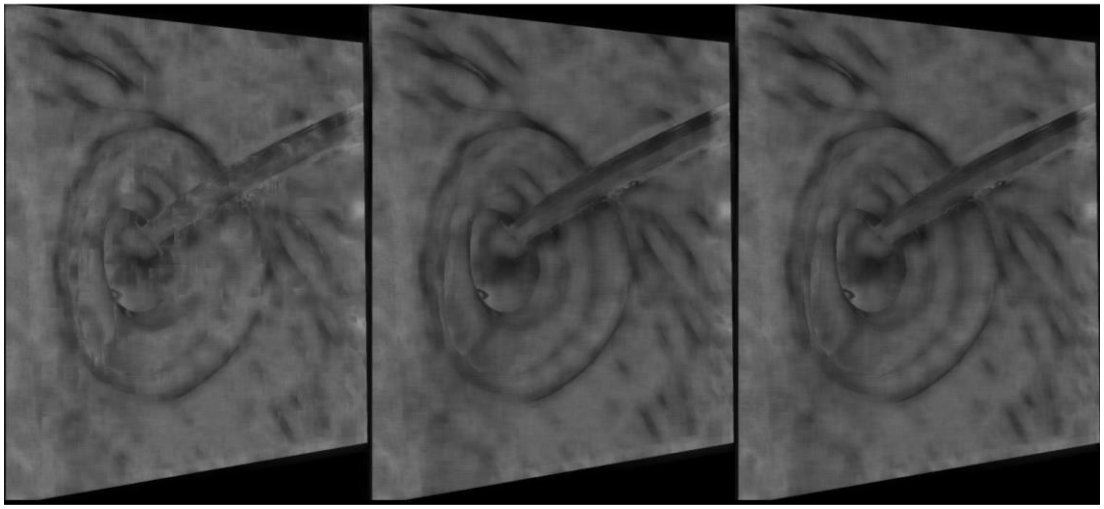

Figure 22 Left View Image Propagation Step [-30 30]

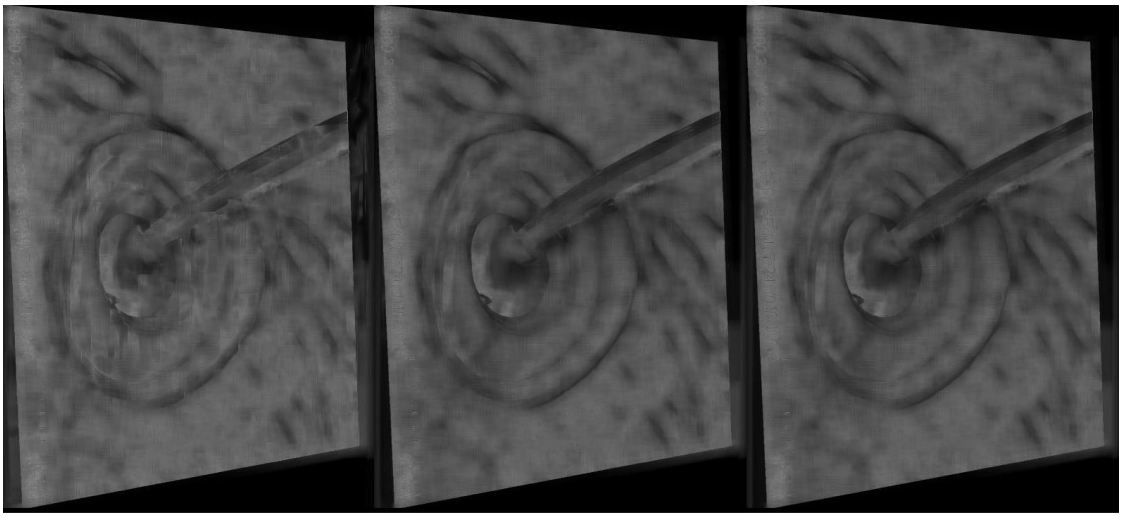

Figure 23 Right View Image Propagation Step [-30 30]

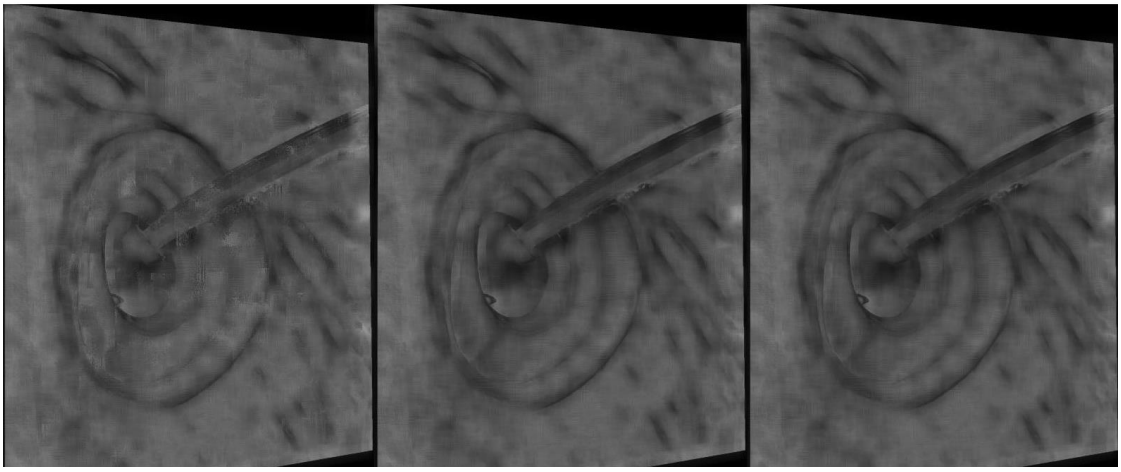

Figure 24 Left View Image Refinement Step [-30 30]

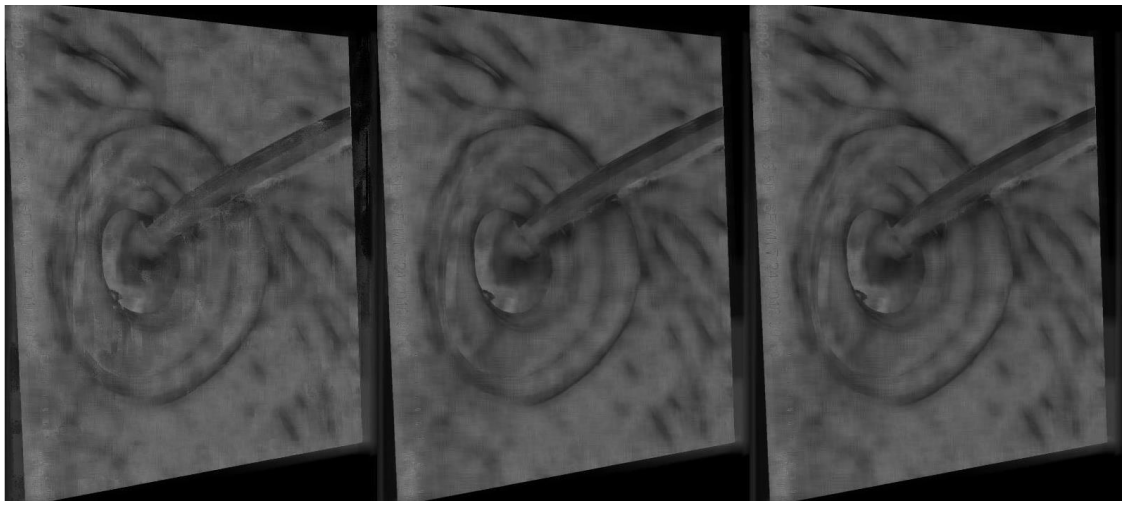

Figure 25 Right View Image Refinement Step [-30 30]

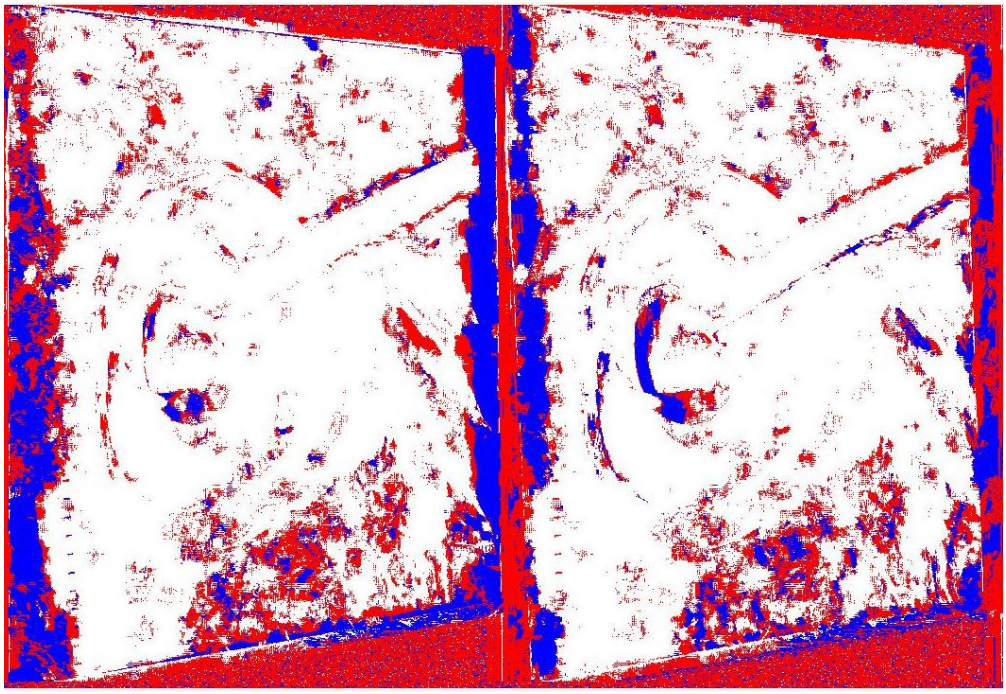

(a) (b)

Figure 26 (a) Left View Image Disparity Map [-30 30]; (b) Right View Image Disparity Map [-30 30]

From the figures shown above it can be clearly seen that the results, when choosing disparity values to be -10 10, are of the better quality than the rest of the two-other set of images. Also choosing -30 30 yields the worst result amongst the three sets. These results directly affect the next step of the approach which is point cloud generation. If the disparity maps are not well defined or have a significant amount of noise in them then the resulting point cloud is a noisy mesh as well.

These results were achieved using the GPU implementation of the Patchmatch Stereo algorithm. The same results can also be achieved by using the CPU version but it is highly time consuming. *Table 2 Comparison Between Computational Time Required by CPU and GPU Implementation of the Patchmatch Stereo Algorithm* provides the comparison in running time

between the CPU and GPU implementation of the Patchmatch Stereo algorithm for different SEM images.

Table 2 Comparison Between Computational Time Required by CPU and GPU Implementation of the Patchmatch Stereo Algorithm; *http://selibcv.org/3dsem/*; *https://www.sciencedirect.com/science/article/pii/S0968432817303128*

SEM Dataset	CPU Implementation	GPU Implementation
Diatom Frustule 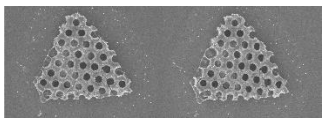	12895.30seconds/ 214.922minutes/ 3.582hours	85.61seconds/ 1.426minutes
Hexagon TEM Copper Grid 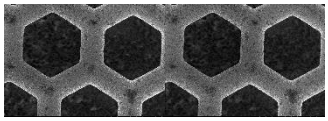	13401.59seconds/ 223.359minutes/ 3.723hours	83.75seconds/ 1.395minutes
Pollen 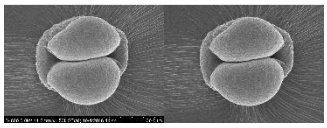	12636.05seconds/ 210.601minutes/ 3.510hours	83.83seconds/ 1.397minutes
Tapetal Cell of Arabidopsis Thaliana 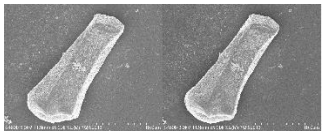	15009.24seconds/ 250.154minutes/ 4.169hours	84.64seconds/ 1.444minutes
Pollen Grain from Brassica Rapa 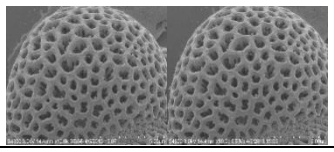	12596.33seconds/ 209.939minutes/ 3.499hours	85.55seconds/ 1.426minutes
Pseudoscorpion 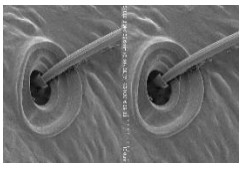	12601.89seconds/ 210.0315minutes/ 3.501hours	82.86sec/ 1.381minutes
Anther 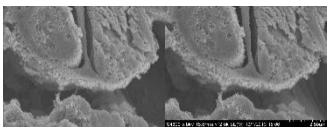	13341.91seconds/ 222.365minutes/ 3.706hours	86.03sec/ 1.434minutes

All the SEM images used here were of the same resolution 640x480 for the sake of fairness of comparison. The disparity values were set to -10 10 for every stereo pair of every dataset. It is clearly seen that the GPU implementation is much faster than the CPU implementation. The computational time difference between the two implementations is huge. It takes the CPU several hours to compute whereas the GPU does the same computation in less than a couple of minutes. If the resolution of the images were to be higher than the one being used or if the disparity values were set to a higher range the computational time would also increase multiple folds specially for the CPU implementation.

The next step is to generate dense point cloud and from that constructing the 3D surface model. To achieve a much better-quality construction the approach adds the feature of point cloud registration. This not only provides better viewing angles for the constructed 3D model but also a much denser surface reconstruction which is the main objective of this research.

2.2.4. Point Cloud Generation and Registration

The results from the previous step are crucial for the point cloud generation. The quality of the point cloud depends on the correctness of the rectification of the stereo images and the disparity map generated by the Patchmatch algorithm. Once the depth map has been received the point cloud can generated using the rectified image that was used as input to the Patchmatch algorithm. An important parameter here is the rotation angle which the user must provide. Usually if the SEM images are taken by the user then the rotation angle is known and that helps in achieving relatively more accurate results.

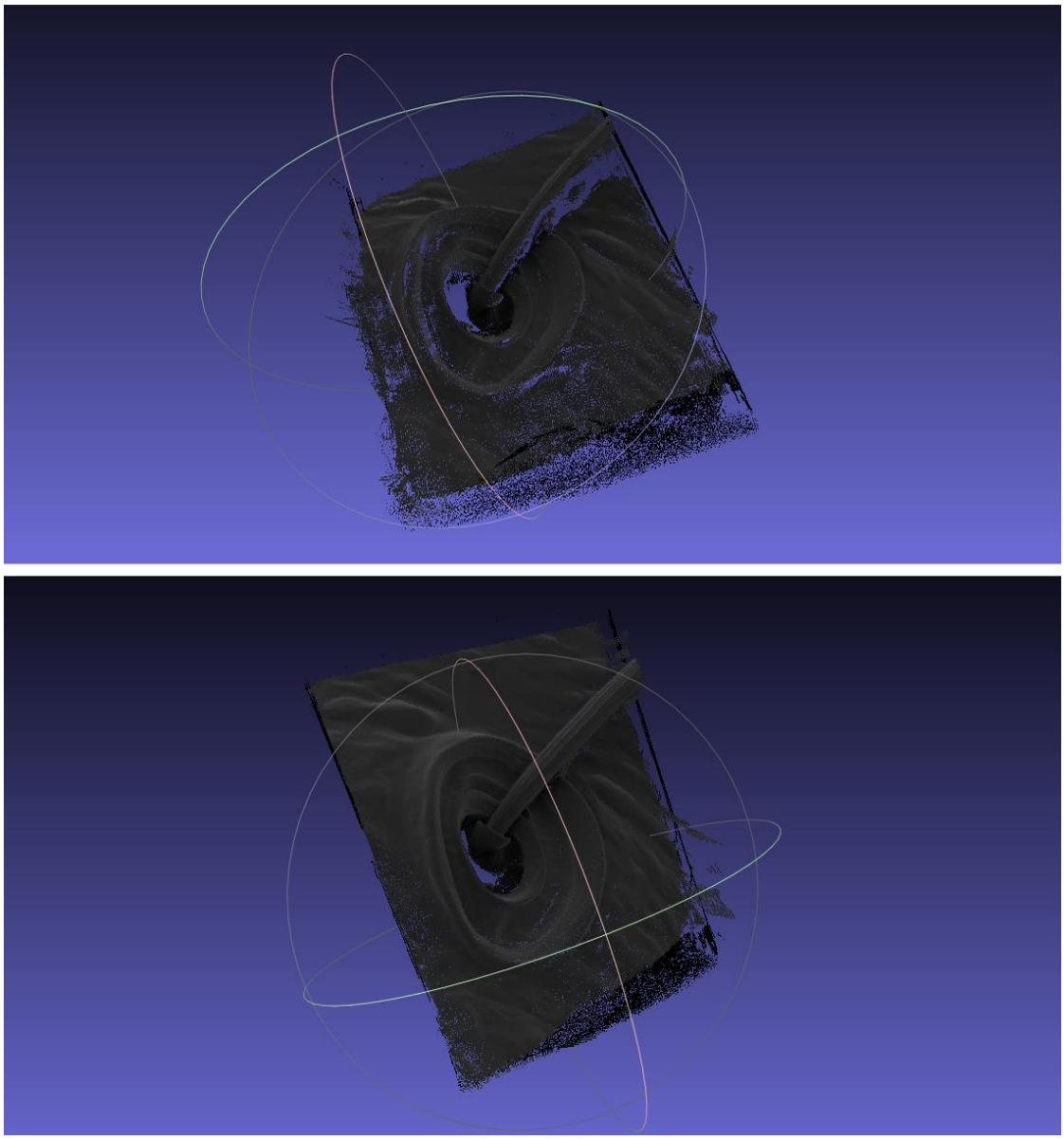

Figure 27 3D Surface Reconstruction of Pseudoscorpion SEM Stereo Pair

This 3D reconstruction is done by using the resulting depth map of the disparity value test set -10 10. Once the 3D construction is done and high detail result is achieved we can move to the next step of registration. But before that the we must generate multiple cloud points from different images of the same dataset. This means that the approach described until now has to be implemented several times (at least 2 times) since registration can be performed on

at least 2 set of point clouds. From *Figure 28 Sparse 3D Reconstructed Pseudoscorpion Surface* below it is seen that from a single stereo pair the reconstruction can be sparse.

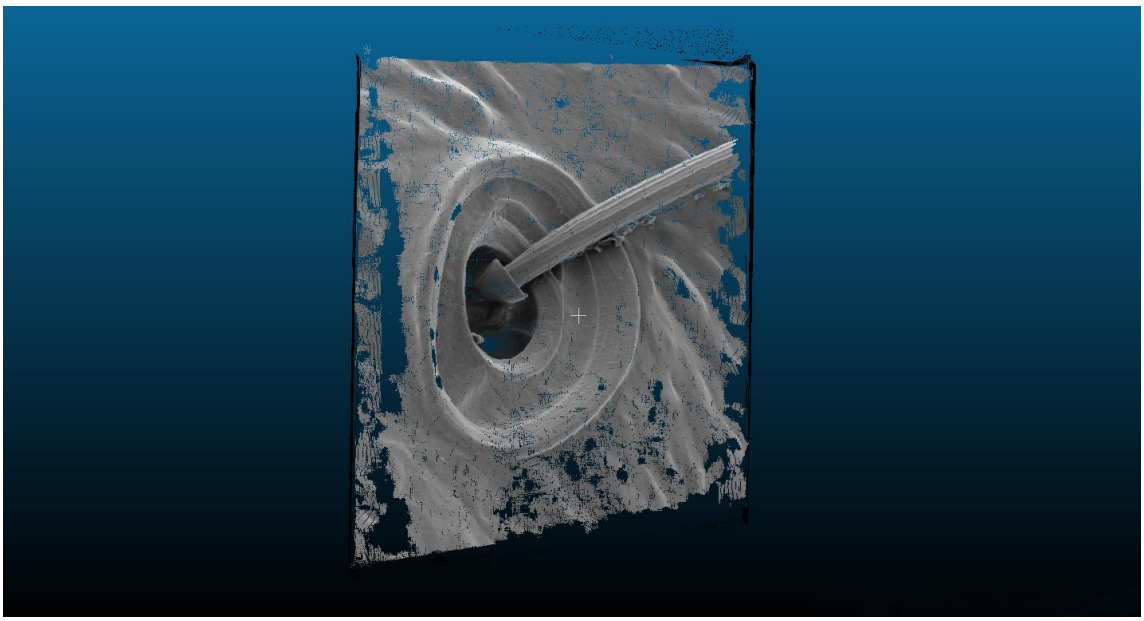

Figure 28 Sparse 3D Reconstructed Pseudoscorpion Surface

This structure is missing details and geometry which is crucial when the interest lies in observing the true shape of the sample. This is where point cloud registration helps and overcomes this obstacle. Point cloud registration is basically using transformation and rotation tools and fitting the two points clouds in such a manner that the key points match with high accuracy. *Figure 29 Dense 3D Surface of Pseudoscorpion using Point Cloud Registration* shows how point cloud registration overcomes this obstacle and provides a much better 3D model to work with.

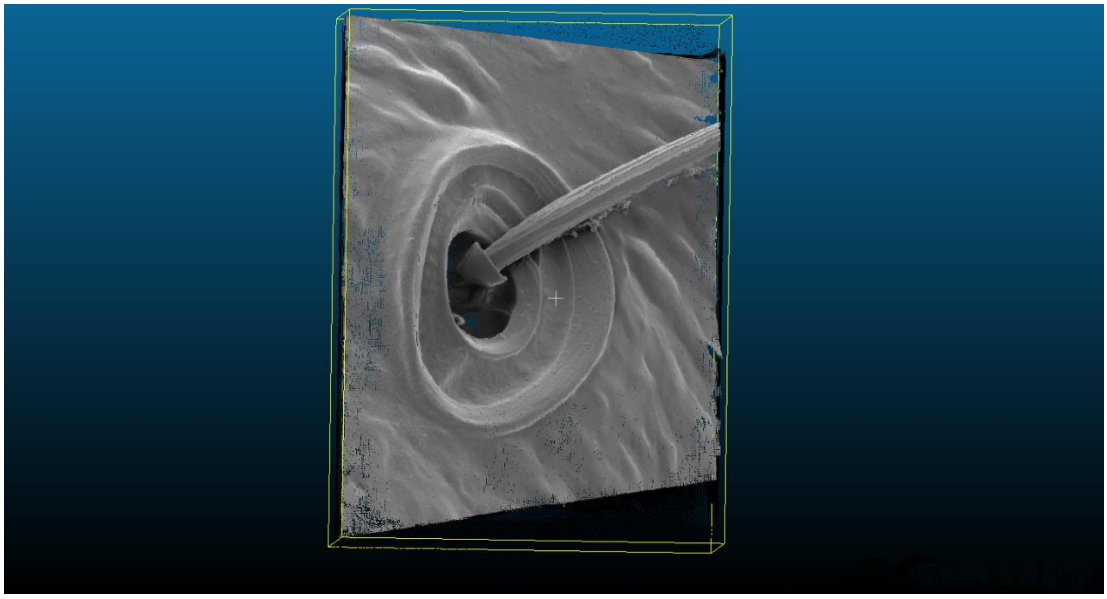

Figure 29 Dense 3D Surface of Pseudoscorpion using Point Cloud Registration

2.3.Results

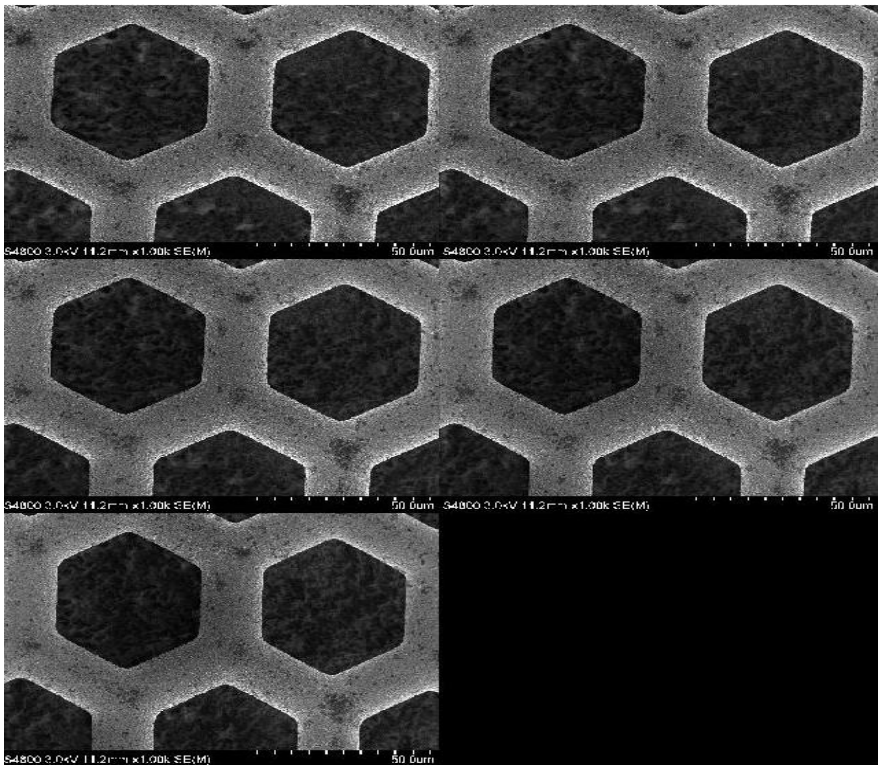

Figure 30 Hexagon TEM Copper Grid Dataset *http://selibcv.org/3dsem/*

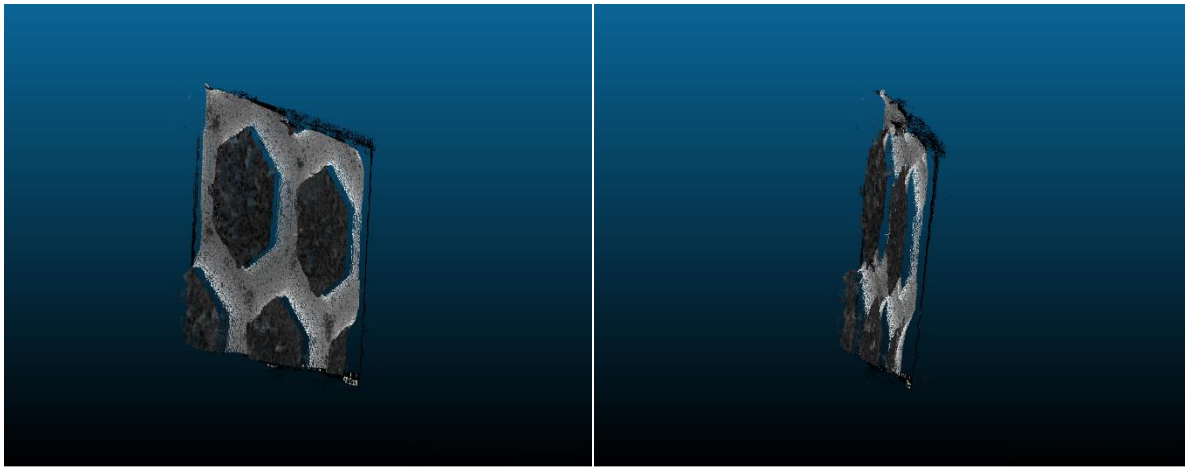

Figure 31 Reconstructed 3D Model without Point Cloud Registration Hexagon TEM Copper Grid Dataset

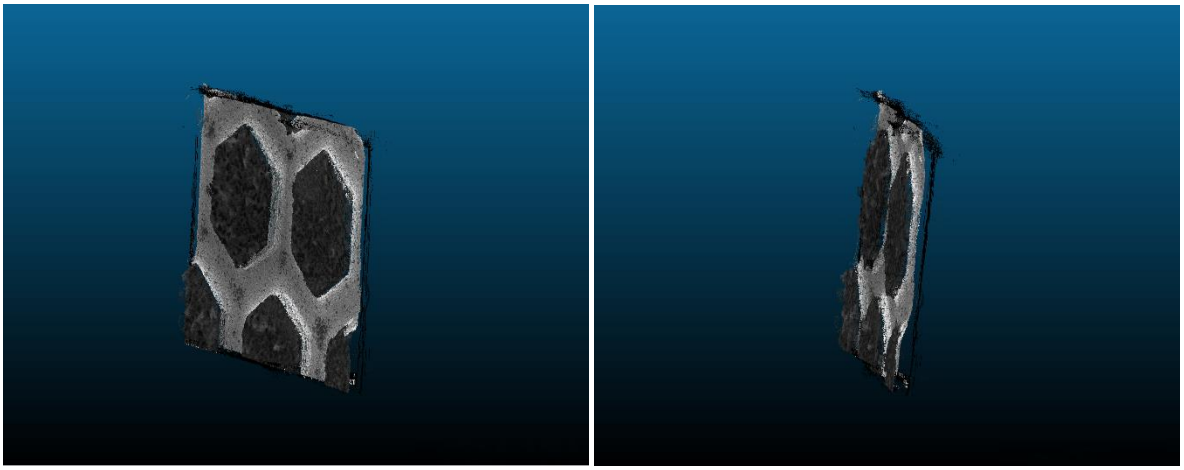

Figure 32 Reconstructed 3D Model with Point Cloud Registration Hexagon TEM Copper Grid Dataset

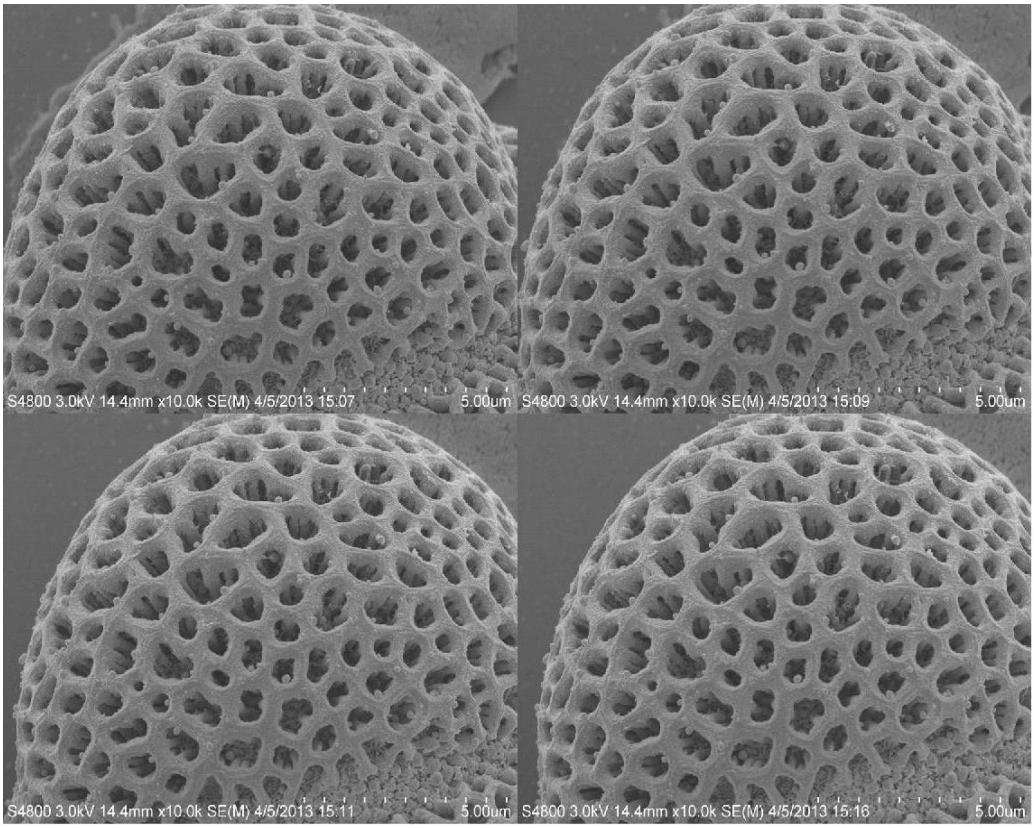

Figure 33 Pollen Grain from Brassica Rapa Dataset *http://selibcv.org/3dsem/*

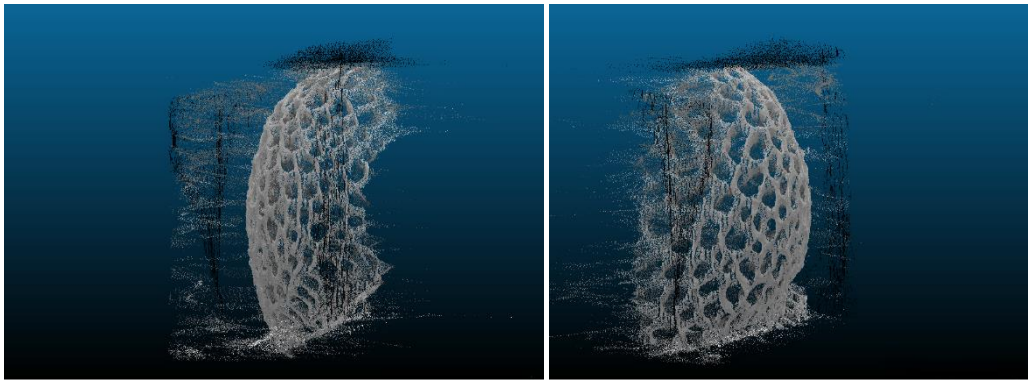

Figure 34 Reconstructed 3D Model without Point Cloud Registration Pollen Grain from Brassica Rapa Dataset

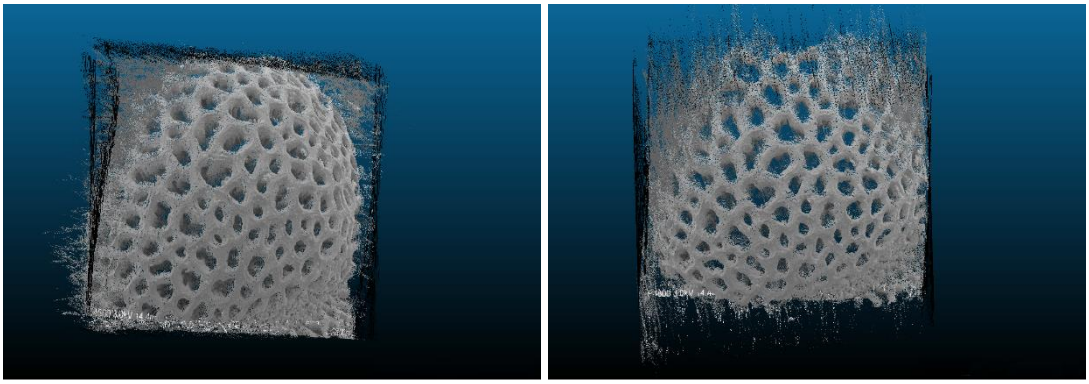

Figure 35 Reconstructed 3D Model with Point Cloud Registration Pollen Grain from Brassica Rapa Dataset

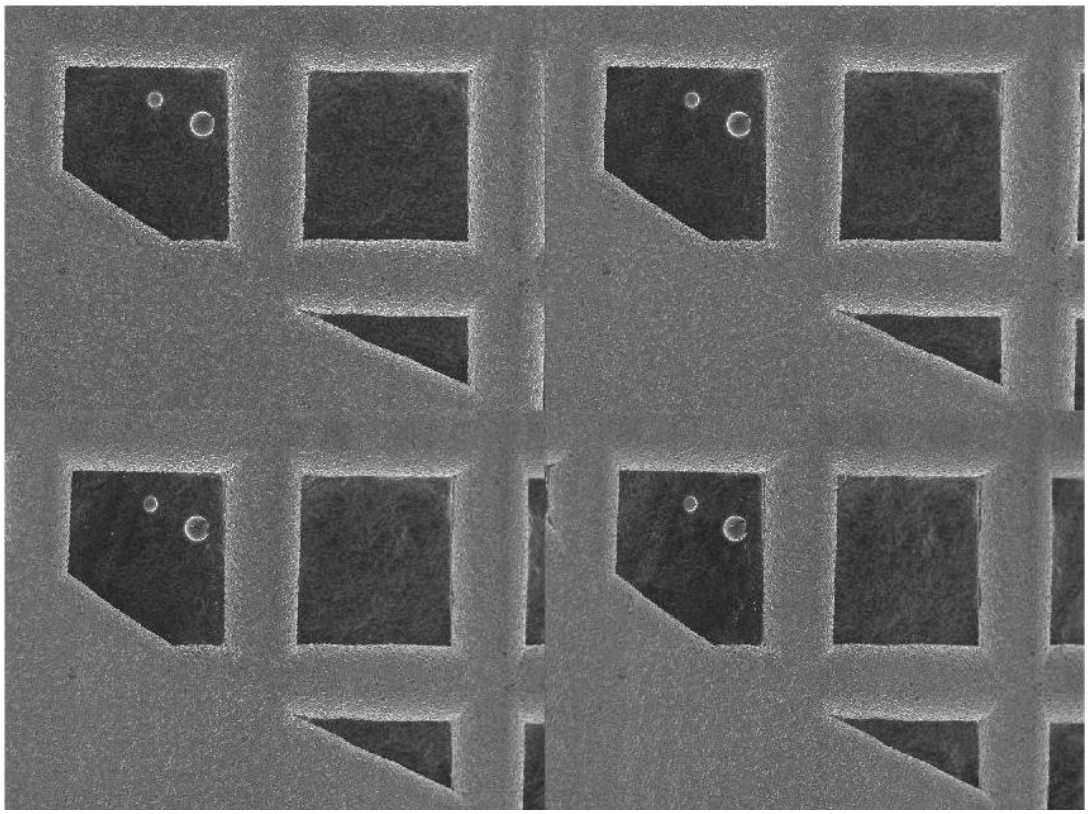

Figure 36 TEM Copper Grid Dataset *http://selibcv.org/3dsem/*

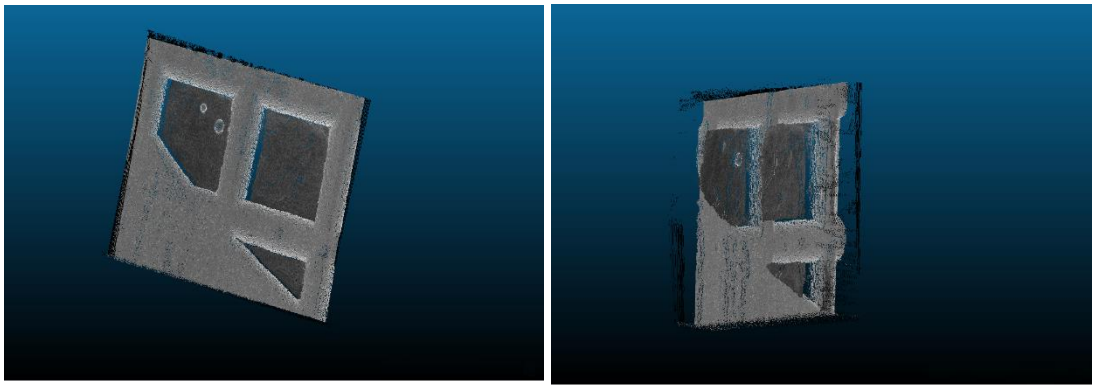

Figure 37 Reconstructed 3D Model without Point Cloud Registration Pollen Grain from TEM Copper Grid Dataset

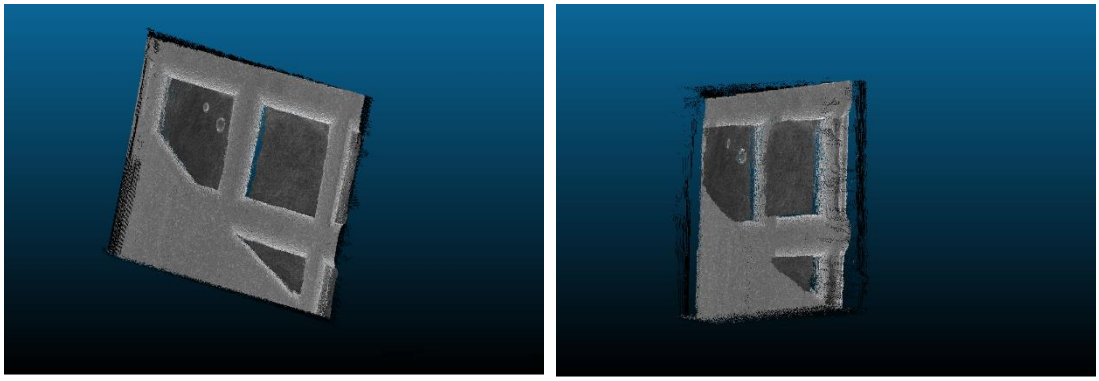

Figure 38 Reconstructed 3D Model with Point Cloud Registration Pollen Grain from TEM Copper Grid Dataset

2.4.Conclusion

The results shown do provide a denser and a much more complete view of the specimen as compared to the traditional 2 image 3D reconstruction. The results are not only dense but also provides more detail and information about the structure and shape of the SEM micrograph.

Even though the results are better than before, this approach has its limitations. Since the approach works locally, that is, it generates the point clouds for every pair of stereo images independently, the errors and noise generated in each point cloud is accumulated in the final result when all the point clouds are registered.

To tackle this problem a global approach method is discussed in the next chapter which instead of working on 2 images at a time, works on the entire data set to find the matches between the images and computing the correspondence between these images within a dataset.

Chapter 3

Global Approach: Regard3D

3.1.Introduction to Regard3D

Regard3D is a structure-from-motion program. That means, it can create 3D models from objects using a series of photographs taken of this object from different viewpoints. The photographs provided as the input must follow this criterion for best possible results:

- Image must be JPEG.
- The focal length as well as the sensor size of the imaging device (for at least some pictures) must be known. This means that:
    - EXIF (metadata) must be present. This provides focal length and camera's make and model.
    - The imaging device (camera) used must be in Regard3D's database.
- Higher the resolution better the resulting reconstruction.
- The photographs should provide a complete view of the object. Any part of the object not visible in more than three pictures will be excluded from the resulting 3D model.

Classic A-KAZE (more precise but slower) and Fast A-KAZE (faster but slightly less good key-points get detected) are two key-point detectors that are used in this approach.

3.2.KAZE Algorithm

KAZE is a multiscale 2D feature detection and description algorithm in nonlinear scale spaces. Previous approaches detect and describe features at different scale levels by building or approximating the Gaussian scale space of an image. However, Gaussian blurring does not respect the natural boundaries of objects and smooths to the same degree both details and noise, reducing localization accuracy and distinctiveness. In contrast, KAZE detects and describes 2D features in a nonlinear scale space by means of nonlinear diffusion filtering. This is done by blurring locally adaptive to the image data, reducing noise but retaining object boundaries, obtaining superior localization accuracy and distinctiveness. Even though the features are somewhat more expensive to compute than SURF due to the construction of the nonlinear scale space, but comparable to SIFT, the results reveal a step forward in performance both in detection and description against previous state-of-the-art methods. The algorithm used in this particular approach is the sped-up version of the KAZE algorithm. It is known as Accelerated KAZE or A-KAZE.

3.3.A-KAZE

A-KAZE or Accelerated KAZE uses a mathematical framework called Fast Explicit Diffusion (FED) to dramatically speed-up the nonlinear scale space computations. A-KAZE achieves comparable results to KAZE (in some datasets) while being much faster than the KAZE.

3.4.Obtaining a 3D Model

To obtain a 3D model, the following steps are performed:

3.4.1. Feature Point Detection

For each image, features also called key-points are detected. Features are points in an object that have a high probability to be found in different images of the same object, for example corners, edges etc. Regard3D uses A-KAZE for this purpose.

For each feature, a mathematical descriptor is calculated. This descriptor has the characteristic that descriptors of the same point in an object in different images (seen from different viewpoints) is similar. Regard3D uses Local Intensity Order Pattern (LIOP) for this purpose.

3.4.2. Key-point Matching

The descriptors from different images are matched and geometrically filtered. The result of this step is a collection of matches between each image pair.

Now "tracks" are calculated. For each feature that is part of a match in an image pair, it is searched also in other images. A track is generated from features if these features satisfy some conditions, for example a track is seen in at least 3 images.

3.4.3. Triangulation

The next step is the triangulation phase. All the matches of all the image pairs are used to calculate:

- The 3D position and characteristic of the "camera", i.e. where each image was shot and the visual characteristics of the camera.

- The 3D position of each "track" is calculated

3.4.4. Densification

The result of the triangulation phase is a sparse point cloud. To obtain a denser point cloud ("densification"), several algorithms can be used.

3.4.5. Surface Generation

- The last step is called "Surface generation". The point clouds are used to generate a surface, either with colored vertices or with a texture.

3.5. Pipeline

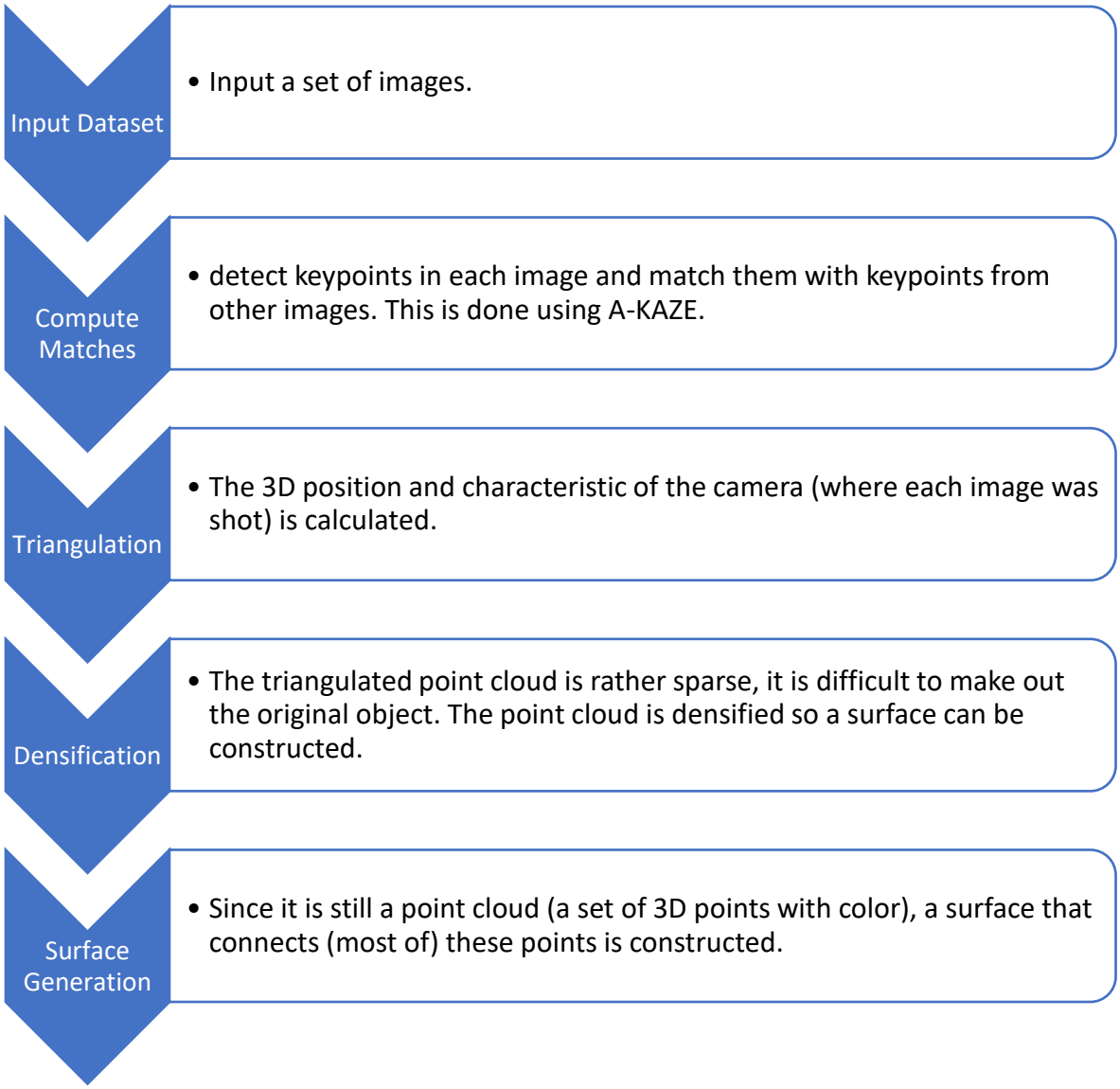
Input Dataset
• Input a set of images.
Compute Matches
• detect keypoints in each image and match them with keypoints from other images. This is done using A-KAZE.
Triangulation
• The 3D position and characteristic of the camera (where each image was shot) is calculated.
Densification
• The triangulated point cloud is rather sparse, it is difficult to make out the original object. The point cloud is densified so a surface can be constructed.
Surface Generation
• Since it is still a point cloud (a set of 3D points with color), a surface that connects (most of) these points is constructed.

3.6. Results

3.6.1. Dataset 1: Kermit

Figure 39 Kermit Dataset 11 Images Montage
https://www.gcc.tu-darmstadt.de/home/proj/mve/

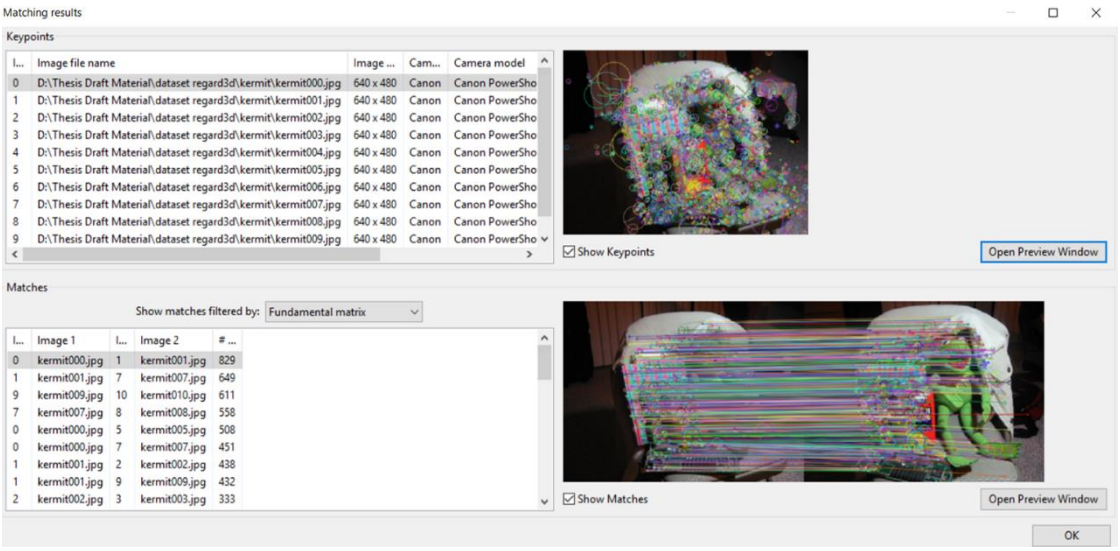

Figure 40 Matching Results from Kermit Dataset

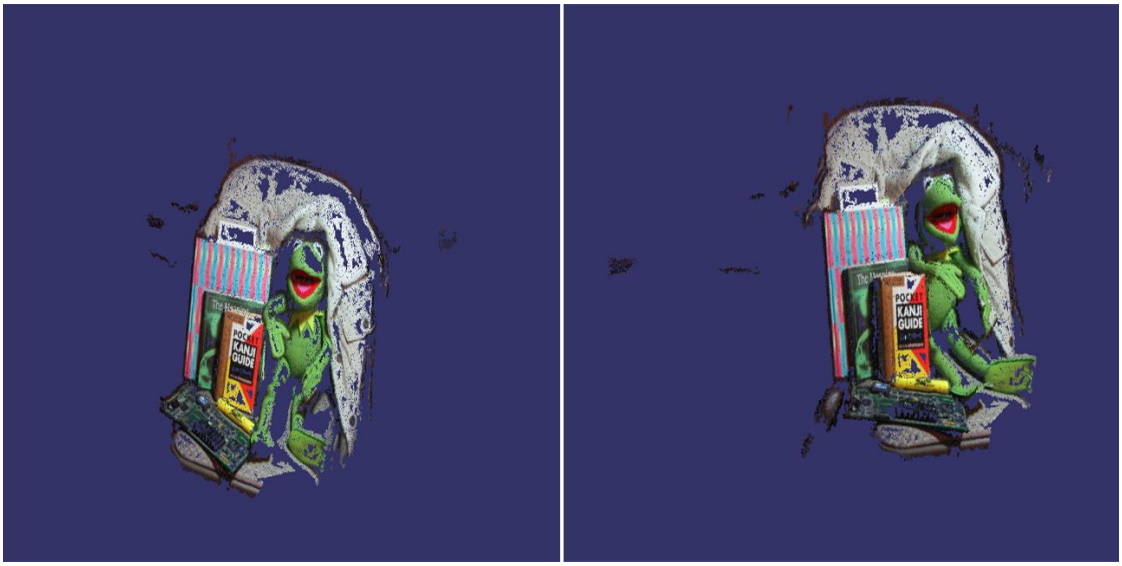

Figure 41 Dense Point Cloud Generation from Triangulated Points Kermit

Figure 42 Generated Surface from 11 Images Kermit Dataset

3.6.2. Dataset 2: Der Hass

Figure 43 Der Hass Dataset 79 Images Montage ***https://www.qcc.tu-darmstadt.de/home/proj/mve/***

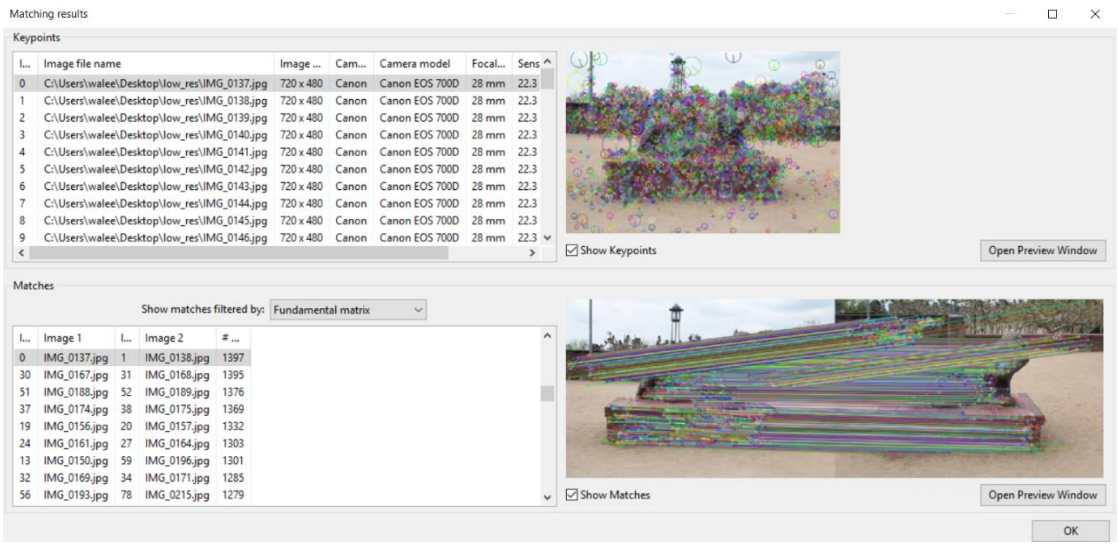

Figure 44 Matching Results From Der Hass Dataset

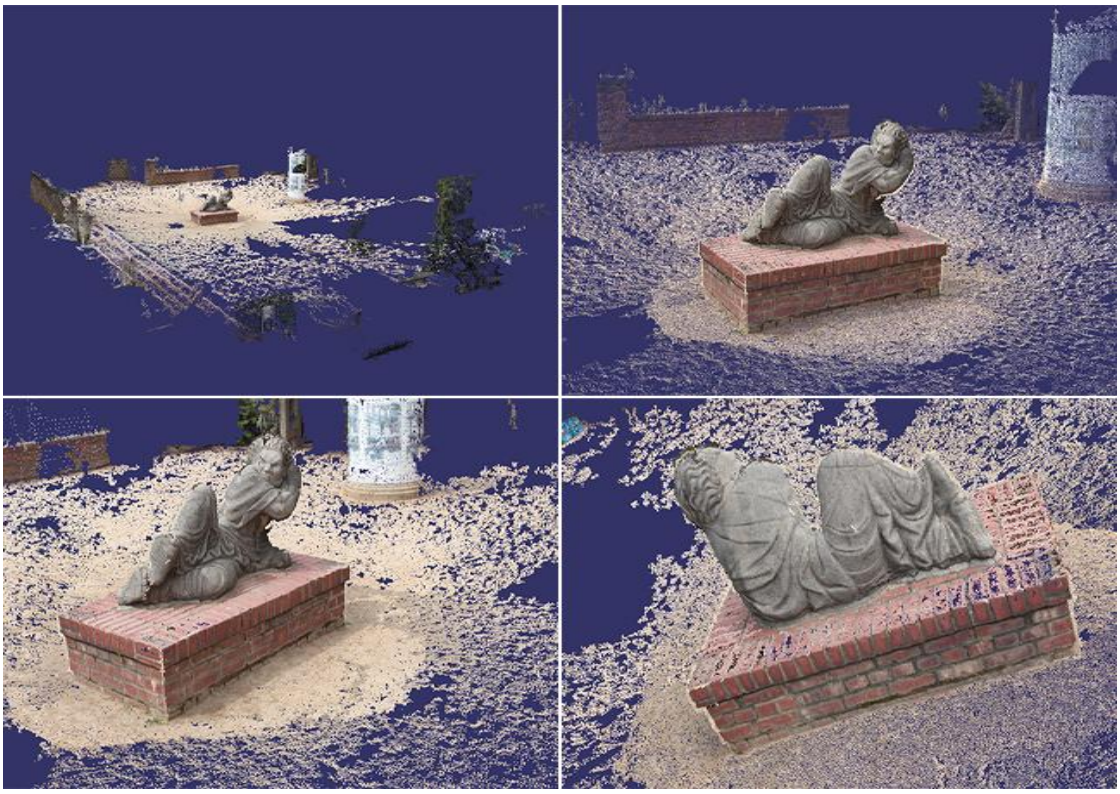

Figure 45 Dense Point Cloud Generation from Triangulated Points Der Hass

Figure 46 Generated Surface from 79 Images Der Hass Dataset

The results shown above were generated using Regard3D running on a system with specifications as follows:

- Processor: Intel® Core™ i5-75300HQ CPU @ 2.50GHz 2.50GHz
- RAM: 8.00 GB

From the table provided below, the time it takes for each step to complete can be seen as well as the total time it takes from finding putative matches to generation of the surface with textures.

Table 3 Step by Step Running Time for Each Dataset

Dataset	Number of Images	Compute Matches	Triangulation	Create Dense Pointcloud	Generate Surface	Total Time
Kermit	11	7.889 sec	2.293 sec	113.227 sec	218.591 sec	342sec
Der Hass	79	475.585sec	59.750sec	1111.190sec	1158.187sec	2804.712sec

Both the datasets used were downscaled to the same image resolution of 640x480 for the sake of relatively faster running time and fair comparison. The settings that were used for each step were set for achieving maximum level detail in the final 3D generated surface model. As shown in *Table 3 Step by Step Running Time for Each Dataset* the total time it took for *Kermit* dataset which consists of 11 images is 342 seconds or 5 minutes and 42 seconds. As for the *Der Hass* dataset which consisted of 79 images the total time required to generate the 3D surface was 2804.712 seconds or 46 minutes and 44.712 seconds.

3.7.Other Low Detail 3D Reconstructions

Figure 47 Low Detail 3D Model Reconstruction of Objects From 3 Images

Figure 48 Low Detail 3D Model Reconstruction of Human Face with 30 Images

3.8. Conclusion

The approach demonstrated above is a general/global 3D reconstruction approach. It can be used to generate 3D model surfaces from any given set of images as long as the camera parameters are known to the user. This provides nicely detailed geometry and textures with fine details. As mentioned in the requirements the higher the input image quality the higher the quality of the resulting 3D model will be. The difference in quality can also be seen from comparing *Figure 42 Generated Surface from 11 Images Kermit Dataset, Figure 46 Generated Surface from 79 Images Der Hass Dataset, Figure 47 Low Detail 3D Model Reconstruction of Objects From 3 Images and Figure 48 Low Detail 3D Model Reconstruction of Human Face From 30 Images.*

Even though the results from this general 3D modeling approach are promising and look good, the actual goal to achieve is 3D surface reconstruction of SEM images is not yet achievable using this approach. Since the intrinsic camera parameters such as the camera's focal length and sensor width are not known, it is not possible to add these values to the camera database for Regard3D. Thus, some modifications and enhancements are to be made before it can be done.

Chapter 4

Conclusions

4.1. Conclusions and Future Work

In this thesis we surveyed different approaches for the 3D surface reconstruction. We discussed the multi-view approach which takes only two images as input at a time. This approach included several steps such as image rectification, using Patchmatch Stereo's GPU implementation and point cloud registration. The approach is useful when dealing with SEM images as can be seen from the figures in the Chapter 2. Since a 3D reconstruction from only two images does not always necessarily provide enough detail and texture, thus the 3D view remains incomplete. With the approach discussed in Chapter 2 we can provide multiple images as input (two at a time) and then generate multiple point clouds for the surface reconstruction. But this pose another obstacle that no view is fully complete view of the specimen under observation.

Point Cloud Registration being the answer to the problem, is used in this thesis to merge those multiple point clouds for the same specimen and creating one complete 3D surface. This registration technique helps not only to provide a more complete view of the specimen but also adds to missing points in other point clouds. During the generation of point clouds some detail in geometry or texture is sometimes left out. This may happen due to faulty feature point detection or some accuracy error during the Patchmatch procedure or can also be because of the noise generated at any given step. With point cloud registration we overlap and fit the

feature points in such a way that it fills these holes and provides a view with small error and more completeness in structure.

Point cloud generation from a pair of images and then registering them is still a local approach to solving the problem thus any error generated in the point cloud generation will accumulate when registering multiple point clouds. This can sometimes lead to results that are not desired and are noisy rather than complete.

To overcome this problem, we discussed the global approach using Regard3D and showed various results generated by the approach. The results were promising in terms of details and large area reconstruction when the intrinsic camera parameters are known. The approach used the Accelerated KAZE algorithm for the feature point extraction and correspondence between the images. It also had multiple libraries backing it up for the purpose of triangulation and surface reconstruction as well as point cloud creation. The end results were impressive but this approach was not quite useful when applied on images whose EXIF or camera details were not known specifically with the SEM images datasets.

Though this is an obstacle for now, but it can be solved by designing such programs that can compute the parameters required by the global approach. With the focal length and rotation angle known this approach can be applied not only to any point and shoot camera but SEM micrographs as well thus providing a complete view (ideally 360-degrees).

Not only this but nowadays much work has been done in the field of computer vision for integrating machine learning/deep learning techniques to the algorithms. This not only improves the overall functionality of the program but also enhances the efficiency and

effectiveness. This new technology used along with the high-power GPUs can revolutionize the field of computer vision by speeding up the processes and providing high quality results.

References

3D SEM. (2015). Retrieved from http://selibcv.org/3dsem

A. P. Tafti, A. B. Kirkpatrick, J. D. Holz, H. A. Owen, & Zeyun Yu. (2015). *3dsem: A 3d microscopy dataset.* Elsevier.

A. P. Tafti, A. B. Kirkpatrick, Z. Alavi, A. Owen, & Zeyun Yu. (2015). *Recent advances in 3d sem surface reconstruction.*

A. P. Tafti, A. Baghaie, A. B. Kirkpatrick, J. D. Holz, H. A. Owen, R. M. DSouza, & Zeyun Yu. (2016). *A comparative study on the application of sift, surf, brief and orb for 3d surface reconstruction of electron microscopy images. Computer Methods in Biomechanics and Biomedical Engineering: Imaging & Visualization.*

A. P. Tafti, J. D. Holz, A. Baghaie, H. A. Owen, M. M. He, & Zeyun Yu. (2016). *3dsem++: Adaptive and intelligent 3d sem surface reconstruction* (Vol. 87). Elsevier.

A. Zolotukhin , I. Safonov, & K. Kryzhanovskii. (2013). 3d reconstruction for a scanning electron microscope. Pattern recognition and image analysis.

Ahmadreza Baghaie, & Heather A. Owen. (2017, September 11). Stereo Scanning Electron Microscopy Dataset.

Ahmadreza Baghaie, Ahmad Pahlavan Tafti, Heather A. Owen, Roshan M. D'Souza, & Zeyun Yu. (2017, April 6). Three-dimensional reconstruction of highly complex microscopic samples using scanning electron microscopy and optical flow estimation.

B. Zitova, & J. Flusser. (2003). *Image registration methods: a survey. Image and vision computing.*

Baghaie, A. (2016). Study of Computational Image Matching Techniques: Improving Our View of Biomedical . Milwaukee.

Baghaie, A., C. Z., A. B., H. A., H. C., R. M., & Z. Y. (2017, December). Slanted support window-based stereo matching for surface reconstruction of microscopic samples.

Caroline A Schneider, Wayne S Rasband, & Kevin W Eliceiri. (2012, June 28). NIH Image to ImageJ: 25 years of image analysis. *Nature Methods*.

CloudCompare. (n.d.). Retrieved from http://www.cloudcompare.org/

Dr. Michael D. Abramoff, Dr. Paulo J. Maghalhaes, & Dr. Sunanda J. Ram. (2004). Image Processing with ImageJ.

Herbert Bay, Andreas Ess, Tinne Tuytelaars, & Luc Van Gool. (2008). Speeded-Up Robust Features (SURF).

Herbert Bay, Tinne Tuytelaars, & Luc Van Gool. (2006). SURF: Speeded Up Robust Features. Springer.

Hiestand, R. (2015). *Regard3D*. Retrieved from http://www.regard3d.org

ImageJ. (1997-2016). Retrieved from https://imagej.nih.gov/ij/

J Bernal, F Vilarino, & J Sánchez. (2010). Feature detectors and feature descriptors: where we are now. *8193*.

K. M. Lee, & C.-C. J. Kuo. (1993). Surface reconstruction from photometric stereo images.

Michael Bleyer, Christoph Rhemann, & Carsten Rother. (n.d.). PatchMatch Stereo - Stereo Matching with Slanted Support Windows.

P. Cignoni, M. Callieri, M. Corsini, M. Dellepiane, F. Ganovelli, & G. Ranzuglia. (2008). MeshLab: an Open-Source Mesh Processing Tool.

SeLibCV. (n.d.). Retrieved from http://selibcv.org/

Simon Fuhrmann, Fabian Langguth, & Michael Goesele. (2014). MVE – A Multi-View Reconstruction Environment.

Tafti, A. P. (2016). *3D SEM Surface Reconstruction: An Optimized, Adaptive, and Intelligent Approach.*

Tafti, A., Kirkpatrick, A., Owen, H., & Yu, Z. (2014). 3D Microscopy Vision Using Multiple View Geometry and Differential Evolutionary Approaches. In *Advances in Visual Computing.* Springer.

Velasco, E. (2013). Scanning Electron Microscope (SEM) as a means to determine dispersibility.

Vernon-Parry, K. (2000). *Scanning electron microscopy: an introduction.* Elsevier.